Solid-State Electronics Vol. 29, No. 8, pp. 791–795, 1986
Printed in Great Britain

0038-1101/86 $3.00 + 0.00
Pergamon Journals Ltd

ANALYSIS OF THE CURRENT–VOLTAGE CHARACTERISTIC OF SOLAR CELLS

D. FUCHS AND H. SIGMUND
Fraunhofer Institut für Festkörpertechnologie, Paul-Gerhardt-Allee 42, 8000 München 60, F.R.G.

(*Received* 16 *July* 1985; *in revised form* 25 *October* 1985)

Abstract—The parameters for the generation–recombination current and diffusion current of a solar cell including series and shunt resistance are determined experimentally by a new method through applying equal current steps to the cell rather than voltage steps. This allows a simple evaluation of the generation–recombination current term in the presence of a low shunt resistance of the cell. In a second measuring cycle the series resistance and the diffusion current term of the cell are determined in a similar way. The presented method is a relative simple and low-cost analysis and it allows a quick and accurate on-line determination of the parameters of the current–voltage characteristic, especially for silicon solar cells.

NOTATION

- A, B constants evaluated by linear regression
- $I(N)$ impressed current [A]
- I_{01} saturation current for generation–recombination [A]
- I_{02} saturation current for diffusion [A]
- I_a current step [A]
- I_d voltage-dependent diffusion current [A]
- I_g voltage-dependent generation–recombination current [A]
- I_{sh} current through the shunt resistance [A]
- n_1 diode-quality factor for generation–recombination
- n_2 diode-quality factor for diffusion
- R_s series resistance [Ω]
- R_{sh} shunt resistance [Ω]
- $V(N)$ measured voltage [V]
- $V_f(N)$ forward voltage at current NI_a
- $V_r(N)$ reverse voltage at current NI_a
- V_f forward voltage [V]
- V_r reverse voltage [V]
- k Boltzmann's Constant ($8.62 \cdot 10^{-5}$ eV/K)
- q Electron charge
- T absolute temperature

1. INTRODUCTION

The current–voltage characteristics of solar cells described by the single-exponential equation, i.e. with only the diffusion current term taken into account, has been carried out using an analytical method by Picciano [1], and using numerical methods by Bryant and Glew [2] as well as by Braunstein *et al.* [3]. The double-exponential equation of solar cells, i.e. taking into account diffusion current and the recombination generation current of the space-charge region, is more closely related to the physical phenomena. There are two numerical methods which are usually employed. In the first method, the diode-quality factor for the recombination–generation current is assumed to be 2 and the diode-quality factor for the diffusion current is assumed as unity, so that the unknown parameters are reduced to four [4, 5]. In the second method, either the shunt resistance is neglected or the diode quality factor for the diffusion current is assumed as unity, and then in both cases the equation is solved numerically to determine five parameters [6, 7]. Both numerical methods are based on the modified least square fit for non-linear equations and require time consuming computer calculations. In this paper we develop a simple and rapid method for determining the parameters of the double-exponential equation for solar cells, including shunt and series resistance and diode-quality factors.

2. ANALYSIS OF THE CURRENT-VOLTAGE CHARACTERISTIC

According to the equivalent circuit of a solar cell, as shown in Fig. 1, the dark-current characteristic is given by [4–8]:

$$I = I_g + I_d + I_{sh}, \tag{1}$$

where I_g is the voltage-dependent generation–recombination current:

$$I_g = I_{01} \cdot \left[\exp\left(\frac{V - I \cdot R_s}{n_1 \cdot V_{th}}\right) - 1\right]. \tag{2}$$

I_d is the voltage-dependent diffusion current:

$$I_d = I_{02} \cdot \left[\exp\left(\frac{V - I \cdot R_s}{n_2 \cdot V_{th}}\right) - 1\right] \tag{3}$$

and I_{sh} is the current flowing over shunt resistance R_{sh}:

$$I_{sh} = \frac{V - I \cdot R_s}{R_{sh}} \tag{4}$$

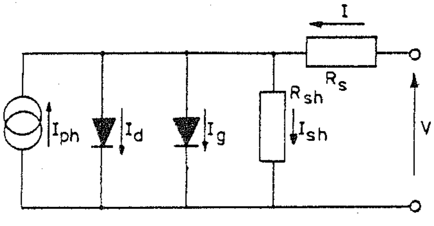

Fig. 1. Solar cell equivalent circuit.

I_{01} — the voltage dependence of I_{01}, especially for reverse voltages, is neglected — and I_{02} are constants and represent the saturation currents of the generation–recombination and diffusion process, respectively; n_1 and n_2 are the diode-quality factors for generation and diffusion, respectively. R_s is the series resistance and $V_{th} = (q/(k \cdot T))$ is the thermal voltage.

The functional dependence of the total current I on the voltage V is determined by six parameters. In order to evaluate these parameters, the current–voltage characteristic is divided into three voltage region, so that certain simplification for eqn (1) are possible.

2.1 *Voltage region I: Reverse characteristic $V \leq -8V_{th}$*

For voltages $V \leq -8V_{th}$, i.e. $V \leq -0.2$ V the exponential terms in eqns (2) and (3) tend towards zero, so that $I_g = -I_{01}$ and $I_d = -I_{02}$. Furthermore in most solar cells, the saturation current I_{02} for the diffusion term is several orders of magnitude smaller than the saturation current I_{01} for the recombination–generation term. Therefore the characteristic is then mainly determined by the I_{sh} term. Because of the low total current I flowing in the reverse direction and the normally small values of the series resistance R_s ($R_s \leq 1\Omega$), the voltage drop $I \cdot R_s$ can also be neglected. Thus, for this voltage region, eqn (1) is reduced to:

$$I = I_g + I_{sh} = -I_{01} + \frac{V}{R_{sh}}. \qquad (5)$$

By applying a current I with fixed current steps I_a in the reverse direction, i.e. $I(N) = N \cdot (-I_a)$, the differential resistance is determined for each pair of $V(N)$, $I(N)$ by:

$$R(N) = \frac{\Delta V}{\Delta I} = \frac{V(N+1) - V(N-1)}{2 \cdot I_a}. \qquad (6)$$

Then, the maximum value of $R(N) = R_{\max}$ is evaluated; and a mean value for the shunt resistance R_{sh} is calculated as follows:

$$R_{sh} = \frac{1}{K - J + 1} \sum_{N=J}^{N=K} R(N)$$

where $R(J)$ is the first taken value from $R(N)$ and $R(K)$ is the last value of $R(N)$ which are located within an interval of $/R_{\max} - \Delta R/$. The value of ΔR can be selected and represents a certain deviation from $R_{\max}$, i.e. $\Delta R/R_{\max}$ should be 2–5%.

2.2 *Voltage region II: $V \leq 15\ V_{th}$*

For voltages $V \leq 15\ V_{th}$, *i.e.* $V \leq 0.4$ V, the diffusion current of a silicon solar cell can normally be neglected [6, 8, 9]. Furthermore, the voltage drop at the series resistance is much smaller than the terminal voltage V of the solar cell. In this case, the current–voltage characteristic is given by:

$$I = I_g + I_{sh} = I_{01} \exp\left(\frac{V}{n_1 \cdot V_{th}}\right) - I_{01} + \frac{V}{R_{sh}}. \qquad (8)$$

By applying a current with N fixed steps in the forward and reverse direction of the cell, so that $V_f(1) \geq 4V_{th}$ and $V_r(1) \leq -8V_{th}$, eqn (8) can be written for the forward direction (index f) as:

$$I(N) = I_{01} \cdot \exp\left(\frac{V_f(N)}{n_1 \cdot V_{th}}\right) - I_{01} + \frac{V_f(N)}{R_{sh}}; \qquad (9)$$

and for the reverse direction (index r) as:

$$-I(N) = -I_{01} + \frac{V_r(N)}{R_{sh}} \qquad (10)$$

[see eqn (5)]. Because equal current steps are applied to the cell in forward and also in reverse direction, the forward and reverse current is given by:

$$I_f = I(N) = N \cdot I_a \quad \text{and} \quad I_r = -I(N) = N \cdot (-I_a),$$

the summation of eqns (9) and (10) then yields:

$$0 = I_{01} \exp\left(\frac{V_f(N)}{n_1 \cdot V_{th}}\right) - 2I_{01} + \frac{V_f(N) + V_r(N)}{R_{sh}} \qquad (11)$$

and the subtraction of eqn (10) from eqn (9) yields:

$$2 \cdot I(N) = I_{01} \exp\left(\frac{V_f(N)}{n_1 \cdot V_{th}}\right) + \frac{V_f(N) - V_r(N)}{R_{sh}}. \qquad (12)$$

Equation (11) or eqn (12) can be used to determine I_{01} and n_1; using eqn (11), one obtains:

$$\ln[-V_f(N) - V_r(N) + K(N)] = \ln(R_{sh} \cdot I_{01}) + \frac{1}{(n_1 \cdot V_{th})} \cdot V_f(N) \qquad (13)$$

with

$$K(N) = \frac{2 \cdot \left(I(N) \cdot R_{sh} - V_f(N)\right)}{\left[\exp\left(\frac{V_f(N)}{2 \cdot V_{th}}\right) - 1\right]}.$$

Setting $y = \ln[-V_f(N) - V_r(N) + K(N)]$ and $x = V_f(N)$, eqn (13) can be written as:

$$y = A + Bx \qquad (13a)$$

where A and B are constants for a given solar cell. They are determined by a linear least-square fit (linear regression):

$$A = \ln(I_{01} \cdot R_{sh}); \qquad I_{01} = \exp(A)/R_{sh} \qquad (13b)$$

$$B = 1/(n_1 \cdot V_{th}); \qquad n_1 = 1/(B \cdot V_{th}). \qquad (13c)$$

In an analog manner, eqn (12) can be applied to determine I_{01} and n_1, also using eqns (13b) and (13c). In this case, the value of y is given by $y = \ln[2 \cdot I(N) \cdot R_{sh} - V_f(N) + V_r(N)]$.

2.3 *Voltage region III: $V \geqslant 15\ V_{th}$*

If $I \geqslant I_g + I_{sh}$ holds, which can easily be proofed using the former results, then the current through the cell is given by:

$$I = I_d = I_{02} \cdot \exp\left(\frac{V - I \cdot R_s}{n_2 \cdot V_{th}}\right). \qquad (14)$$

The series resistance R_s must be determined first, in order to evaluate I_{02} and n_2. In the literature several methods have been investigated. Most of them are based on illuminated current–voltage characteristics measurements [8, 10–12]. For sufficient accuracy in determining R_s, high illumination levels (several suns) are necessary. A further possibility for the determination of R_s has been given by Araujo [4] and Wolf *et al.* [6] and involves the method of minimizing the standard deviation for a given set of measured and calculated current values. Here we use the dark-characteristic measurement of a solar cell in order to evaluate R_s. With eqn (14), one obtains:

$$\ln I - \ln I_{02} = (V - I \cdot R_s)/(n_2 \cdot V_{th}). \qquad (15)$$

Subtracting eqn (15) for two pairs of V and I, one obtains after some rearranging:

$$\frac{I_2 - I_1}{\ln(I_2/I_1)} = -\frac{n_2 \cdot V_{th}}{R_s} + \frac{1}{R_s} \cdot \frac{V_2 - V_1}{\ln(I_2/I_1)} \qquad (16)$$

where $I_2 = I(N)$ and $I_1 = I(N - 1)$ are the applied currents and $V_2 = V(N)$ and $V_1 = V(N - 1)$ the measured voltages. Again, a least square fit (linear regression) can be made, with the variables $y = (I_2 - I_1)/\ln(I_2/I_1)$ and $x = (V_2 - V_1)/\ln(I_2/I_1)$. The series resistance is given from the gradient of the linear regression line:

$$R_s = 1/B \qquad (17a)$$

or from the intersection of the regression line with the y-axis with $n_2 = 1$:

$$R_s = -n_2 \cdot V_{th}/A = -V_{th}/A. \qquad (17b)$$

Consequently from one iteration process one obtains two values for R_s, one for $n_2 \neq 1$ [eqn (17a)] and a second one, assuming $n_2 = 1$ [eqn (17b)].

If the condition $I(N) \gg I_g(N) + I_{sh}(N)$ is not satisfied, then I_2 and I_1 are substituted by $I_2 = I(N) - I_g(N) - I_{sh}(N)$ and $I_1 = I(N - 1) - I_g(N - 1) - I_{sh}(N - 1)$ and R_S can be estimated with eqns (16)–(17b). The values for $I_g(N)$ and $I_{sh}(N)$ can be calculated with the known parameters for I_g and I_{sh}, with $V = V(N) - I(N)R_{so}$. For two measured pairs of V and I in the high-current region, one obtains from eqn (16) with $n_2 = 1$ and setting $R_s = R_{so}$:

$$R_{so} = \frac{V_2 - V_1}{I_2 - I_1} - V_{th}\frac{\ln(I_2/I_1)}{I_2 - I_1}. \qquad (18)$$

The value of R_{so} can be considered as a rough approximation for R_s.

As soon as a proper value of R_s is found, I_{02} and n_2 may be determined. We start with eqns (1) and (4), and obtain:

$$\ln\{I(N) - I_g(N) - I_{sh}(N)\}$$
$$= \ln I_{02} + (V(N) - I(N) \cdot R_s/(n_2 \cdot V_{th})). \qquad (19)$$

A linear regression [see eqn (13a)] can be carried out with the variables $y = \ln\{I(N) - I_g(N) - I_{sh}(N)\}$ and $x = V(N) - I(N) \cdot R_s$. This yields:

$$A = \ln I_{02}; \qquad I_{02} = \exp(A)$$

$$B = 1/(n_2 \cdot V_{th}); \qquad n_2 = 1/(B \cdot V_{th}). \qquad (20b)$$

3. EXPERIMENTAL

Figure 2 shows the block diagram of the experimental arrangement. A personal computer (Hewlett Packard 86) is used to control the measurements and to process the measured data. As shown in Fig. 2 the current is applied by a programmable current source (Keithley 220) and the resulting voltage is measured by programmable digital multimeter (Keithley 195). The current source can apply a current from 1 pA up to 100 mA, with steps between 0.5 pA and 50 μA. In the effective voltage range (± 2 V) used, the digital multimeter has a resolution of 10 μV. A floppy-disc unit is connected to the computer by a HP-IB interface as an additional mass-storage unit. The sample is kept at constant temperature during measurement.

The first step in the measurement procedure is to determine the size of the smallest current step I_a. With the same number of steps in the reverse and forward direction, the pairs of values $(I(N), V(N))$ are measured (region I and II). With these data the parameters of the shunt resistance R_{sh}, the generation–recombination current term I_{01} and the quality factor n_1 are calculated.

Following this, data are measured, starting at a current level I which satisfies the condition $I \geqslant I_g + I_{sh}$. The current I is here increased with a factor C, i.e. $I(N) = C \cdot I(N - 1)$, with $C = 1.1$–1.5 (region III). With these data and the results of the previous calculations for R_{sh}, I_{01} and n_1, the remaining parameters for the series resistance R_s, the diffusion current I_{02} and the diode quality factor for the diffusion current n_2 are determined. A simplified flow-chart diagram of the program is shown in Fig. 3.

4. RESULTS AND DISCUSSION

As examples only two cells of several investigated solar cells which had been differently processed will be discussed in the following. Cell A was a monocrystalline, 10 Ωcm resistivity, n^+–p–p^+ cell with an anti-reflection coating. Cell B was a polycrystalline, 2 Ωcm resistivity, n^+–p-cell without an anti-reflection coating. Both cells had an area of 4 cm^2. During measurement, the temperature was kept constant at

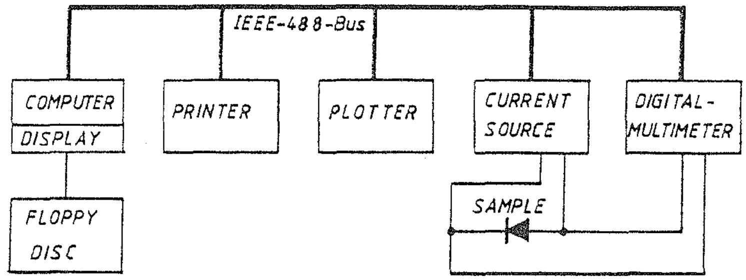

Fig. 2. Block diagram of the experimental arrangement.

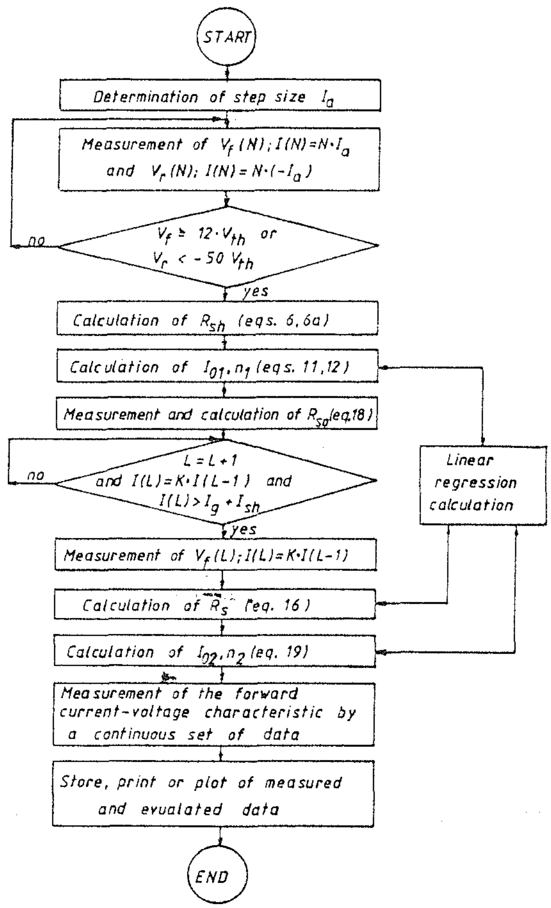

Fig. 3. Simplified flow chart diagram of the computer program.

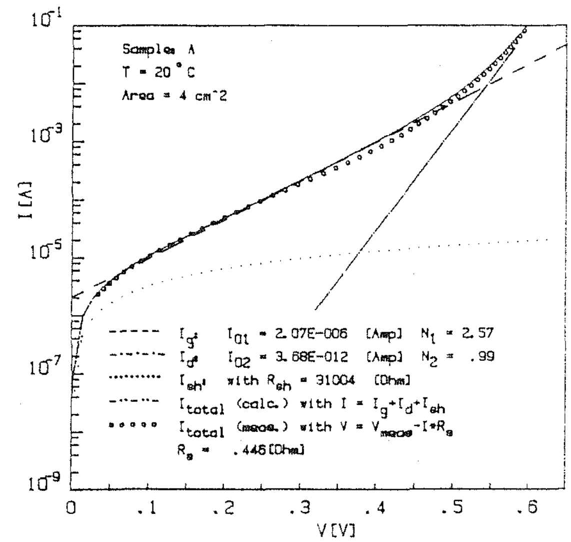

Fig. 4. Current–voltage characteristic of Cell A.

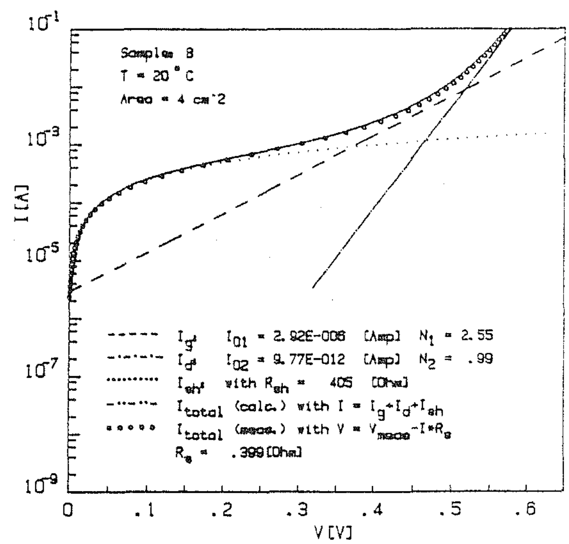

Fig. 5. Current–voltage characteristic of Cell B.

$T = 20°C$. Figures 4 and 5 show the analyzed currents I_g, I_d, I_{sh} and $I_{tot} = I_g + I_d + I_{sh}$ as well as the measured current–voltage characteristic. These figures illustrate the good agreement between the calculated and measured characteristics. In Table 1 all analyzed values of the solar cell parameters are given.

To confirm the results obtained for the six parameters to describe the current-voltage characteristic of a cell, additional measurements under illuminated condition were made, i.e. the dependence of the open-circuit voltage V_{oc} on the short circuit current I_{sc} of the cell under varying illumination level were measured and these V_{oc} and I_{sc} values were compared with those computed from the I–V characteristic using the analyzed parameters. Under illumination of the cell a photocurrent I_{ph} (Fig. 1) is generated. This photocurrent has to be added to eqn (1). For $V = V_{oc}$ and $I = O$ (open circuit

Table 1. Calculated parameters of the investigated cells

PARAMETERS	CELL A	CELL B
R_{sh}	31 000 Ohm	400 Ohm
I_{01} ; n_1		
according to eq. 11	$1.91\cdot10^{-6}$A ; 2.47	$2.92\cdot10^{-6}$A ; 2.55
" eq. 12	$2.07\cdot10^{-6}$A ; 2.57	$2.68\cdot10^{-6}$A ; 2.74
R_s		
according to eq. 16	0.446 Ohm	0.399 Ohm
" eq.16 (n_2 = 1)	0.449 "	0.357 "
" ref. [4]	0.489 "	0.398 "
I_{02}		
according to eq. 19	$3.68\cdot10^{-12}$A	$9.77\cdot10^{-12}$A
" ref. [4]	$4.98\cdot10^{-12}$A	$8.22\cdot10^{-12}$A
n_2 according to eq. 19	0.99	0.99

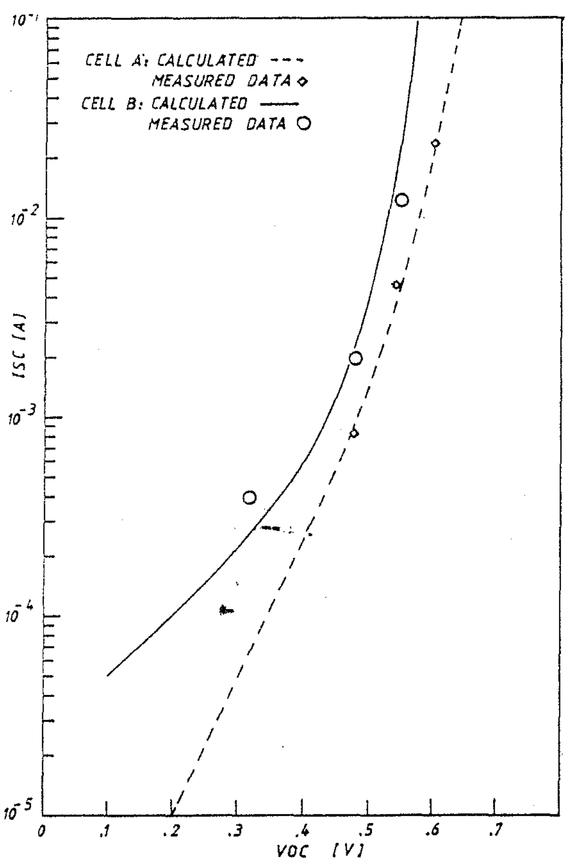

Fig. 6. V_{oc}-I_{sc}-characteristic of cells A and B calculated with the evaluated parameters and compared with measured values.

condition) one yields:

$$0 = I_{01}\left[\exp\left(\frac{V_{oc}}{n_1 \cdot V_{th}}\right) - 1\right] + I_{02}\left[\exp\left(\frac{V_{oc}}{n_2 V_{th}}\right) - 1\right] + \frac{V_{oc}}{R_{sh}} - I_{ph} \quad (21)$$

and for $V = 0$ and $I = I_{sc}$ (short current condition) one gets

$$I_{sc} = I_{01}\left[\exp\left(\frac{-I_{sc} \cdot R_s}{n_1 V_{th}}\right) - 1\right] + I_{02}\left[\exp\left(\frac{-I_{sc} \cdot R_s}{n_2 V_{th}}\right) - 1\right]\frac{I_{sc} R_c}{R_{sh}} - I_{ph}\,. \quad (22)$$

From eqns (21) and (22) the relation between I_{sc} and V_{oc} of a dark current analyzed cell can be calculated and compared with measured data for I_{sc} and V_{oc} of the cell.

As shown in Fig. 6 there is an excellent agreement between measured and calculated data for the open circuit voltage V_{oc} and the short circuit current I_{sc}.

5. CONCLUSIONS

The procedure shown to analyze the I–V characteristic of a solar cell is suitable to determine the parameters of the generation–recombination and diffusion current including the shunt and series resistance of the cell. By this method time-consuming calculations are not necessary and the measurements as well as the analysis of the characteristic are made on-line. This is possible because current steps are applied to the cell rather than voltage steps. By this technique it is further possible to determine the parameters by linear regression. The dark current characteristic of the investigated silicon solar cells could be well described by the model, which may be further proofed by the measured and calculated $I_{sc} - V_{oc}$ relation of the cells.

REFERENCES

1. W. T. Picciano, *Energy Conversion* **9**, 1–6 (1968).
2. F. J. Bryant and R. W. Glew, *Energy Conversion* **14**, 129–133 (1975).
3. A. Braunstein, J. Bany and J. Appelbaum, *Energy Conversion* **17**, 1–6 (1977).
4. G. L. Araujo, E. Sanchez and M. Marti, *Solar Cells* **5**, 199–204 (1982).
5. E. S. Rittner, *J. Energy* **5**, 9–14 (1981).
6. M. Wolf, G. T. Noel and R. J. Stirn, *IEEE Trans. Electron Dev.* **ED-24**, 419–428 (1977).
7. R. J. Stirn, *Proc. 9th IEEE Photovoltaic Spec. Conf.* 72–82 (1972).
8. M. Wolf and H. Rauschenbach, *Advanced Energy Conversion* **5**, 455–479 (1963).
9. E. S. Rittner, *J. Energy*, **1**, 9–17 (1977).
10. K. Rajkaran and J. Shewchun, *Solid-St. Electron.* **22**, 193–197 (1979).
11. J. Cape and S. W. Zehr, *Proc. 14th IEEE Photovoltaic Spec. Conf.* 449–551 (1980).
12. G. L. Araujo and E. Sanchez, *IEEE Trans. Electron Dev.* **ED-29**, 1511–1513 (1982).

PHYS 555

Solid-State Electronics Vol. 29, No. 3, pp. 329–337, 1986
Printed in Great Britain.

0038-1101/86 $3.00 + .00

A COMPARATIVE STUDY OF EXTRACTION METHODS FOR SOLAR CELL MODEL PARAMETERS

D. S. H. Chan, J. R. Phillips and J. C. H. Phang
Department of Electrical Engineering, National University of Singapore, Kent Ridge, Singapore 0511

(*Received* 27 *April* 1984; *in revised form* 1 *May* 1985)

Abstract—A comparative study of three methods for extracting solar cell parameters of the single-diode lumped-circuit model is presented. The methods compared are the curve-fitting method, an iterative 5-point method and a recently proposed analytical 5-point method. Parameter values were extracted using these three methods from experimental characteristics collected from two silicon cells over a range of illuminations and temperatures. The results show that the curve-fitting method can often give erroneous parameter values and the reasons for the errors are discussed. The 5-point methods are found to be reliable and accurate in situations where the model is a good approximation of cell performance. The analytical 5-point method, however, has the added advantage of simplicity. It is also found that for the cell measured, the single diode model is valid at illuminations above one-half AM1 but gives non-physical parameter values at lower illumination.

NOTATION

- σ standard deviation of current deviation
- ϵ area deviation as defined in eqn (16)
- ΔArea area deviation as defined in eqn (15)
- $(I_{exp})_j$ experimental current value at jth data point
- I_m current at maximum power point
- I_{ph} photocurrent
- I_s diode saturation current
- I_{sc} short circuit current
- $(I_{th})_j$ theoretical current value at jth data point
- k Boltzmann's constant
- n diode quality factor
- N number of data points
- q electronic charge
- R_s lumped series resistance
- R_{sh} lumped shunt resistance
- R_{sho} reciprocal of slope at short circuit point
- R_{so} reciprocal of slope at open circuit point
- T temperature (K)
- $(V_{exp})_j$ experimental voltage value at jth data point
- V_m voltage at maximum power point
- V_{oc} open circuit voltage
- V_T kT/q
- $(V_{th})_j$ theoretical voltage value at jth data point

1. INTRODUCTION

The determination of solar cell model parameters from experimental data is important in the design and evaluation of solar cells. While a number of methods have been suggested for measuring the series resistance of a solar cell, other parameters, which are also important, have not received the same amount of attention, and few direct methods of extracting these other parameters have been proposed.

The most commonly used method for measuring the series resistance of a solar cell was first proposed by Wolf and Rauschenbach[1]. This involves measuring the characteristic of a cell at two different illuminations. Two advantages go with this method: firstly, it does not require prior knowledge of the other model parameters such as junction ideality factor, reverse saturation current and shunt resistance, provided that the parameters remain constant at the two illuminations and operating points. Secondly, the method can be used as a small-signal technique[2]. The method of Rajkanan and Shewchun[3], using data from a dark and an illuminated characteristic, gives a value of R_s based on assumptions that parameter values do not change with illumination. We have found that model parameters do change with illumination and that large errors may result. The method of Araujo *et al.*[4], using the area under an I–V curve, has many implicit assumptions which renders it accurate only for very low R_s and high illuminations[2].

A method for the direct measurement of shunt resistance was proposed recently[5]. This involved the measurement of open circuit voltage and short circuit current at very low illuminations such that the dark diode current would be negligible compared with the dark shunt current. The other methods of extracting the parameters in the single diode model involve either lengthy curve-fitting procedures or iterative calculations[6–11]. Otterbein *et al.*[7] minimised the sum of the squares of the residuals and thus arrived at a set of values of R_s, n and I_s. However, shunt resistance was neglected. Araujo[8] used a similar technique in fitting his data to a two diode model which also neglected R_{sh}. Other authors[12] have suggested that curve fitting can give erroneous parameter values and ought to be used with care.

Kennerud[9] and later Charles[10] proposed another iterative method based on fitting a theoretical curve to the experimental voltage and slope at the open circuit point, the maximum power point (V_m, I_m), and the current and slope at the short circuit point. This will be referred to as the exact five point method throughout this paper. Although this method does not try to fit the model to every point of the curve, it does generate a curve that fits the experimental data well, enabling all the five model parameters to be extracted. There are however practical difficulties in measuring the short-circuit and open-circuit slopes accurately. We have recently proposed a method [13], similar in principle to Kennerud's, that provides a direct analytical extraction of the five parameters using the experimental data points V_{oc}, I_{sc}, V_m, I_m, R_{so} and R_{sho}.

In this paper, a comparative study is presented of parameter values obtained over a range of illuminations from 3 extraction methods, namely the exact and the analytical 5 point methods and a curve-fitting method using a more appropriate minimisation criterion than that used by most other authors.

2. THEORY OF METHOD

2.1 *The analytical five point method*

The single diode lumped parameter equivalent circuit of a solar cell is given in Fig. 1. At a given illumination, the current–voltage relationship is given by

$$I = I_{ph} - \left(\frac{V + IR_s}{R_{sh}}\right) - I_s\left(\exp\frac{V + IR_s}{nV_T} - 1\right). \tag{1}$$

It has been shown [9] that the circuit parameters I_{ph}, R_s, R_{sh}, I_s and n at a particular temperature and illumination can be computed from the values V_{oc}, I_{sc}, V_m, I_m, R_{so} and R_{sho} (Fig. 2) measured from the I–V characteristic.

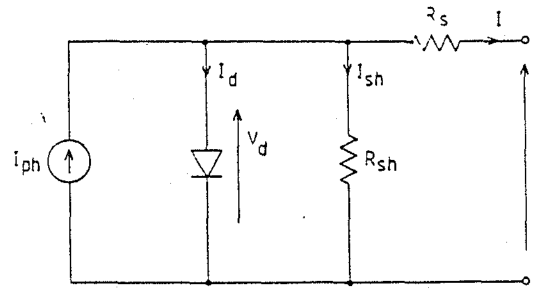

$$I_d = I_s \exp\left(\frac{V_d}{nV_T} - 1\right)$$

Fig. 1. The single diode model for solar cells.

The following non-linear equations can be derived from the circuit model:

$$I_s\left(\exp\frac{V_{oc}}{nV_T} - \exp\frac{I_{sc}R_s}{nV_T}\right) - I_{sc}\left(1 + \frac{R_s}{R_{sh}}\right) + \frac{V_{oc}}{R_{sh}} = 0. \tag{2}$$

$$(R_{so} - R_s)\left(\frac{1}{R_{sh}} + \frac{I_s}{nV_T}\exp\frac{V_{oc}}{nV_T}\right) - 1 = 0 \tag{3}$$

$$\frac{1}{R_{sh}} - \frac{1}{R_{sho} - R_s} + \frac{I_s}{nV_T}\exp\frac{I_{sc}R_s}{nV_T} = 0 \tag{4}$$

$$I_s\exp\frac{V_{oc}}{nV_T} + \frac{V_{oc} - V_m}{R_{sh}} - \left(1 + \frac{R_s}{R_{sh}}\right)I_m - I_s\exp\frac{V_m + R_sI_m}{nV_T} = 0. \tag{5}$$

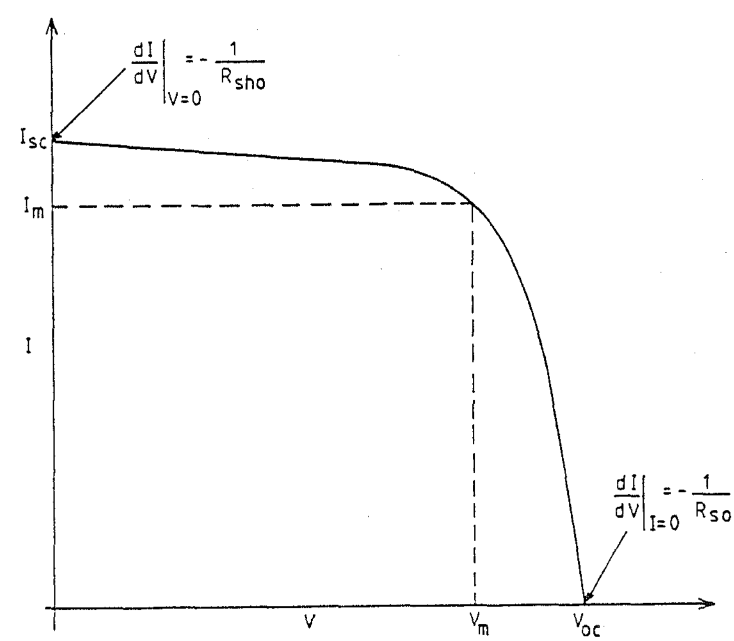

Fig. 2. Input parameters for the 5-point methods.

Kennerud[9] and Charles *et al.*[10] have shown that the four parameters, n, I_s, R_s and R_{sh} may be determined by using the Newton–Raphson method of solving the non-linear simultaneous equations (2)–(5). However, this method requires extensive computation and also good initial guesses for the iterations to converge. In many cases, it was found that there are difficulties in determining these guesses in order to solve the equations[11]. Thus, there is a need for analytical expressions that will enable the direct determination of I_{ph}, n, I_s, R_s and R_{sh}.

By considering the parameter values for typical cells and making some approximations[13], eqns (2)–(5) can be simplified to the following:

$$I_s \exp \frac{V_{oc}}{nV_T} - I_{sc} + \frac{V_{oc}}{R_{sh}} = 0 \qquad (6)$$

$$(R_{so} - R_s)\frac{I_s}{nV_T} \exp \frac{V_{oc}}{nV_T} - 1 = 0 \qquad (7)$$

$$R_{sh} = R_{sho} \qquad (8)$$

$$I_s \exp \frac{V_{oc}}{nV_T} + \frac{V_{oc} - V_m}{R_{sh}} - I_m - I_s \exp \frac{V_m + R_s I_m}{nV_T} = 0. \qquad (9)$$

From these equations an analytical expression for n in terms of the measured parameters is

$$n = \frac{V_m + R_{so} I_m - V_{oc}}{V_T \left\{ \ln\left(I_{sc} - \frac{V_m}{R_{sho}} - I_m \right) - \ln\left(I_{sc} - \frac{V_{oc}}{R_{sh}} \right) + \left(\frac{I_m}{I_{sc} - \frac{V_{oc}}{R_{sho}}} \right) \right\}}. \qquad (10)$$

I_s, R_s and I_{ph} may then be found from

$$I_s = \left(I_{sc} - \frac{V_{oc}}{R_{sh}} \right) \exp\left(-\frac{V_{oc}}{nV_T} \right) \qquad (11)$$

$$R_s = R_{so} - \frac{nV_T}{I_s} \exp\left(-\frac{V_{oc}}{nV_T} \right) \qquad (12)$$

$$I_{ph} = I_{sc}\left(1 + \frac{R_s}{R_{sh}} \right) + I_s\left(\exp \frac{I_{sc} R_s}{nV_T} - 1 \right). \qquad (13)$$

The errors present in the parameter values obtained from the analytical expressions in eqns (10)–(12) were computed[13], and found to be within 1% for R_s in the range 1–150 mΩ and R_{sh} in the range 30–3000 Ω.

2.2 *Curve fitting techniques*

The advantage of the curve fitting method is that all the points in the curve are used, resulting in a higher level of confidence in the parameter values obtained. Many workers (e.g. [8], [12]) have used the standard deviation of the current as the fitting criterion, where the standard deviation is defined by

$$\sigma = \sqrt{ \frac{1}{N} \sum_{j=1}^{N} \left(\frac{(I_{th})_j - (I_{exp})_j}{(I_{exp})_j} \right)^2 }. \qquad (14)$$

The use of this criterion tends to give a very good fit to the part of the curve near the open circuit region at the expense of the quality of fit in the short-circuit region. This arises from the fact that relative current errors tend to be much larger near the open-circuit region where the dI/dV slope is steepest. For a similar reason the use of voltage deviation as a fitting criterion gives a good fit at the short circuit region at the expense of the quality of fit at the open circuit region. Another undesirable feature is that the value of σ may be heavily dependent on the distribution of data points in the characteristic, thus undermining its usefulness as a yardstick of comparison between qualities of fit of different characteristics.

In this work the area, "ΔArea," between the theoretical and experimental characteristics in the quadrant of interest is used as the criterion of fit (see Fig. 3). Using the trapezoidal rule this area can be given by

$$\Delta \text{Area} = \sum_{j=1}^{N-1} \text{ABS}\left\{ \frac{\left[(I_{th})_j + (I_{th})_{j+1} - (I_{exp})_{j+1} - (I_{exp})_j \right]\left((V_{exp})_{j+1} - (V_{exp})_j \right)}{2} \right\}. \qquad (15)$$

Minimisation of ΔArea would give the best fit evenly over the entire characteristic. We can extend this by suggesting a parameter ϵ to describe the quality of fit between the theoretical and experimental curves. This parameter can be obtained by normalising ΔArea by the total area under the experimental I–V curve. Thus

$$\epsilon = \frac{\Delta \text{Area}}{\sum_{j=1}^{N-1} \frac{\left[(I_{exp})_j + (I_{exp})_{j+1} \right]\left[(V_{exp})_{j+1} - (V_{exp})_j \right]}{2}}. \qquad (16)$$

This parameter ϵ is independent of the distribution of points and provides a good basis for comparing

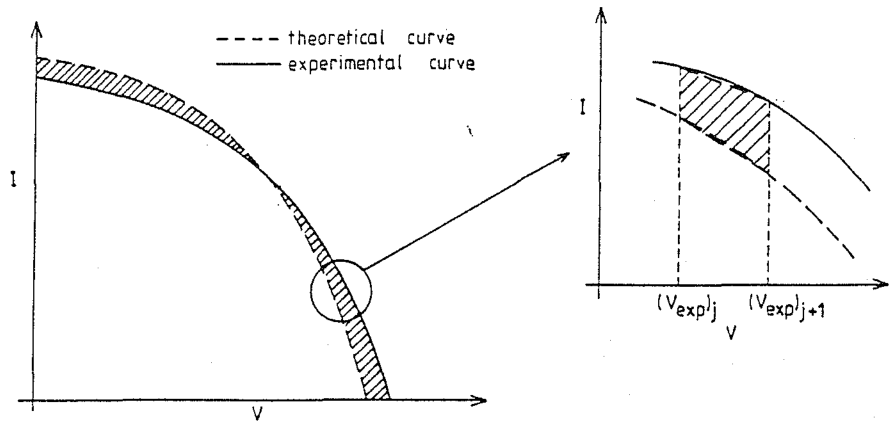

Fig. 3. The area criterion of fit.

qualities of fit of different circuit models to an overall characteristic.

3. EXPERIMENTAL METHODS

Current–voltage characteristics of solar cells were measured through a microcomputer based data logging system utilising 12 bit A/D and D/A converters and a Keithley 227 current source as a variable load. About 60 points were logged for each I–V characteristic and the process of measurement took about 1 sec. The device under test was mounted on a large temperature controlled aluminium block and was illuminated by a tungsten lamp powered by a d.c. current source. The combination of temperature control and high-speed data collection ensured that the characteristics were measured at a constant temperature known to within 1°C. In order to minimise the effect of the wire resistance on the measurements, a four wire technique was used. A block diagram of the measurement system is shown in Fig. 4.

The slopes of the characteristic at short circuit $(=\frac{1}{R_{sho}})$ and open circuit $(=\frac{1}{R_{so}})$ conditions were measured using an a.c. technique. For R_{so}, a 100 Hz

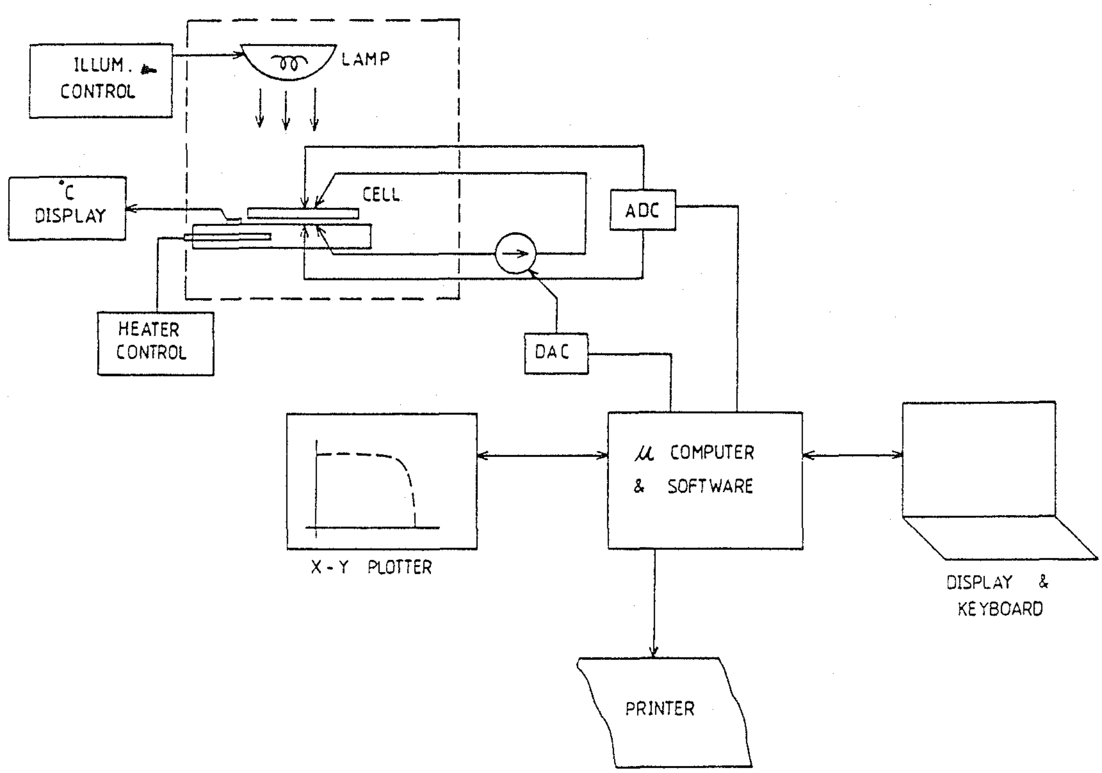

Fig. 4. The experimental measurement system.

small signal current of typically 2 mA amplitude was applied to the open circuit solar cell and the resulting ac voltage of typically 1 mV was measured with a digital meter. For the measurement of R_{sho}, the device was maintained in the short circuit condition by varying the current source to maintain approximately zero voltage across the device terminals. In practice, this was difficult to achieve as very small changes in the short-circuit current caused large changes in the voltage. While this condition was maintained, an a.c. current source of typically 0.1 mA amplitude was superimposed on the d.c. short circuit current, and the resulting a.c. voltage of 50–100 mV was monitored. The values of R_{so} and R_{sho} measured using the a.c. method were compared with those taken from the I–V characteristic. There was general agreement between these two methods, but the a.c. method always gave a more consistent result as would be expected. However the determination of R_{sho} was possible only to an accuracy of about 10%.

4. DISCUSSION OF RESULTS

Two 3 inch cells with efficiencies of 11% and 14%, respectively, were measured at different illuminations and temperatures: Cell #1, with an efficiency of 14%, was measured at 50°C over a range of illuminations, while cell #2 was measured at above half AM1 at 60°C and 90°C. From the data collected, the five parameters of the single diode model were extracted for each characteristic in three ways for comparison purposes:

a) By the analytical 5 point method using eqns (8), (10)–(13).

b) By the exact 5 point method in which eqns (2)–(5) are iteratively solved.

c) By curve fitting techniques, i.e. finding the set of parameters which gave a minimum value for ΔArea. The results of these methods are presented in Table 1 together with the values of ϵ as defined in eqns (16). A comparison of these results shows that the differences between the analytical and the exact 5 point methods are negligible, confirming the results of the error analysis in[13]. A comparison of the results from the analytical and curve fitting methods showed that I_{ph}, n, I_s, from the two methods were virtually identical. However, there were differences in the values of R_s and R_{sh} which were significant at low illuminations. Despite these differences, these results indicate that for short circuit currents above 600 mA (or roughly half AM1), the analytical 5 point method provides parameter values which are similar to that given by the time consuming curve fitting method. The values of n are virtually identical and the values of I_s differed by not more than 5%, while the values of R_s differed by not more than 13%. The large difference in the value of R_{sh} are noted, and the causes for this will be discussed.

In order to investigate the problem in recovering R_{sh}, theoretical I–V characteristics were computed using the parameters obtained by the different meth-

Table 1. Extracted parameter values using 3 different extraction methods

Cell	Temp	DATA CODE		I_{sc} (A)	I_{ph} (A)	n	I_s (μA)	R_s (mΩ)	R_{sh} (Ω)	ε (%)
#1	50°C	SN1	ANAL. 5 PT.	0.7766	0.7766	1.379	1.341	10.32	142.0	0.1570
			EXACT 5 PT.	0.7766	0.7767	1.379	1.338	10.35	142.9	0.1588
			CURVE FIT	0.7766	0.7775	1.379	1.333	9.095	71.00	0.08489
#1	50°C	SN2	ANAL. 5 PT.	0.7112	0.7112	1.359	1.087	10.92	140.0	0.1905
			EXACT 5 PT.	0.7112	0.7112	1.359	1.085	10.95	140.7	0.1916
			CURVE FIT	0.7112	0.7121	1.359	1.072	9.716	69.39	0.09305
#1	50°C	SN3	ANAL. 5 PT.	0.6049	0.6049	1.353	0.9787	10.38	148.5	0.2200
			EXACT 5 PT.	0.6049	0.6049	1.352	0.9765	10.42	149.2	0.2212
			CURVE FIT	0.6049	0.6056	1.353	0.9674	8.789	76.53	0.09803
#1	50°C	SN4	ANAL. 5 PT	0.5519	0.5519	1.345	0.9089	9.733	152.0	0.1755
			EXACT 5 PT.	0.5519	0.5199	1.345	0.9069	9.781	152.6	0.1766
			CURVE FIT	0.5519	0.5524	1.345	0.9006	8.561	81.23	0.1112
#1	50°C	SN5	ANAL. 5 PT.	0.4993	0.4993	1.358	0.9998	9.751	157.0	0.2174
			EXACT 5 PT.	0.4993	0.4993	1.358	0.9976	9.809	157.7	0.2194
			CURVE FIT	0.4993	0.5002	1.358	0.9919	6.237	73.95	0.1024
#1	50°C	SN6	ANAL. 5 PT.	0.4500	0.4500	1.366	1.021	6.913	161.0	0.1885
			EXACT 5 PT.	0.4500	0.4500	1.365	1.019	6.981	161.8	0.1897
			CURVE FIT	0.4500	0.4504	1.365	1.018	3.661	88.86	0.1058
#1	50°C	SN7	ANAL. 5 PT.	0.3915	0.3915	1.363	0.9686	4.335	165.0	0.1966
			EXACT 5 PT.	0.3915	0.3915	1.362	0.9660	4.415	165.7	0.1560
			CURVE FIT	0.3915	0.3919	1.362	0.9713	0.6384	98.8	0.1050

Table 1. *Continued*

Cell	Temp	DATA CODE		I_{sc} (A)	I_{ph} (A)	n	I_s (μA)	R_s (mΩ)	R_{sh} (Ω)	ε (%)
#1	50°C	SN8	ANAL. 5 PT.	0.3500	0.3500	1.369	1.014	4.192	170.0	0.2463
			EXACT 5 PT.	0.3500	0.3500	1.369	1.011	4.295	170.8	0.2480
			CURVE FIT	0.3500	0.3500	1.369	1.004	-0.2852	90.22	0.1268
#1	50°C	SN9	ANAL. 5 PT.	0.2993	0.2993	1.388	1.155	0.6731	173.0	0.2601
			EXCAT 5 PT.	0.2993	0.2993	1.387	1.152	0.8056	173.9	0.2624
			CURVE FIT	0.2993	0.2998	1.386	1.134	-6.154	94.20	0.1480
#1	50°C	SN10	ANAL. 5 PT.	0.2498	0.2498	1.396	1.219	-2.370	175.0	0.3457
			EXACT 5 PT.	0.2498	0.2498	1.396	1.215	-2.184	176.0	0.3488
			CURVE FIT	0.2498	0.2502	1.394	1.181	-9.657	102.7	0.1411
#1	50°C	SN11	ANAL. 5 PT.	0.2007	0.2007	1.405	1.228	-7.464	178.0	0.3003
			EXACT 5 PT.	0.2007	0.2007	1.404	1.223	-7.172	179.0	0.3023
			CURVE FIT	0.2007	0.2007	1.404	1.220	-18.38	128.5	0.07785
#1	50°C	SN12	ANAL. 5 PT.	0.1501	0.1500	1.467	1.907	-22.02	176.0	0.3602
			EXACT 5 PT	0.1501	0.1500	1.466	1.900	-21.50	177.4	0.3663
			CURVE FIT	0.1501	0.1503	1.465	1.861	-35.31	129.3	0.1945
#1	50°C	SN13	ANAL. 5 PT.	0.09981	0.09981	1.547	3.093	-59.83	178.0	0.2999
			EXACT 5 PT.	0.09981	0.09978	1.547	3.092	-58.73	180.1	0.3170
			CURVE FIT	0.09981	0.1000	1.546	3.058	-77.16	147.1	0.2031
#1	50°C	SN14	ANAL. 5 PT.	0.04818	0.04818	1.671	5.530	-147.7	199.0	0.4549
			EXCAT 5 PT.	0.04818	0.04818	1.672	5.581	-145.4	203.3	0.4989
			CURVE FIT	0.04818	0.04830	1.671	5.563	-162.3	203.9	0.2664
#2	60°C	B 706A	ANAL. 5 PT.	0.7002	0.7002	1.504	5.964	21.59	18.80	0.2033
			EXACT 5 PT.	0.7002	0.7010	1.500	5.798	22.05	18.85	0.2348
			CURVE FIT	0.7002	0.7019	1.499	5.745	19.98	15.11	0.1105
#2	60°C	B 806A	ANAL. 5 PT.	0.7994	0.7994	1.502	6.138	24.86	18.77	0.2717
			EXACT 5 PT.	0.7994	0.8005	1.499	5.994	25.22	18.82	0.2834
			CURVE FIT	0.7994	0.8016	1.499	5.942	22.54	14.55	0.0900
#2	60°C	B 906A	ANAL. 5 PT.	0.9050	0.9050	1.559	9.913	22.33	18.85	0.1665
			EXACT 5 PT.	0.9050	0.9061	1.556	9.716	22.64	18.95	0.2121
			CURVE FIT	0.9050	0.9068	1.555	9.669	21.37	15.30	0.0971
#2	90°C	B 709A	ANAL. 5 PT.	0.7163	0.7163	1.407	32.23	28.30	15.74	0.1791
			EXACT 5 PT.	0.7163	0.7176	1.405	31.84	28.81	16.00	0.2468
			CURVE FIT	0.7163	0.7184	1.405	31.56	26.49	12.80	0.0804
#2	90°C	B 809A	ANAL. 5 PT.	0.8315	0.8315	1.441	42.50	27.62	15.35	0.1559
			EXACT 5 PT.	0.8315	0.8330	1.441	42.49	27.99	15.70	0.1672
			CURVE FIT	0.8315	0.8335	1.441	42.16	27.08	13.35	0.0666
#2	90°C	B 909A	ANAL. 5 PT.	0.9356	0.9356	1.490	62.57	26.80	15.07	0.1297
			EXACT 5 PT.	0.9356	0.9373	1.491	63.11	27.09	15.59	0.1150
			CURVE FIT	0.9356	0.9375	1.491	63.06	26.51	13.99	0.0782

ods. The theoretical characteristic and the corresponding experimental curve for one illumination level are shown in Fig.5(a). The current error $I_{th} - I_{exp}$ is also plotted in Fig.5(b) for both analytical and curve-fitting methods against device voltage. It was found that all the characteristics at varying illuminations had similarly shaped error plots. Two components of current error can be distinguished: one is a random scatter caused by noise in the experimental data, the other is a systematic error which can be attributed to the deviation of the characteristics of this device from ideal single diode model behaviour. It can also be observed that the analytical method has very small errors at the short circuit, open circuit and maximum power regions. The good fit that is achieved at the short circuit region is the result of setting R_{sh} to be equal to the slope of the characteristic at short circuit. The curve fitting method on the other hand gives a lower overall current error at the expense of accuracy in the short circuit region. This lower overall error is obtained by altering the values of R_s and R_{sh}, and in some cases to the extent that R_{sh} is half the value of R_{sho}.

It can be argued, however, that while curve fitting produces a lower value of ϵ, it does not give a more accurate value for R_s and R_{sh}. From the analysis

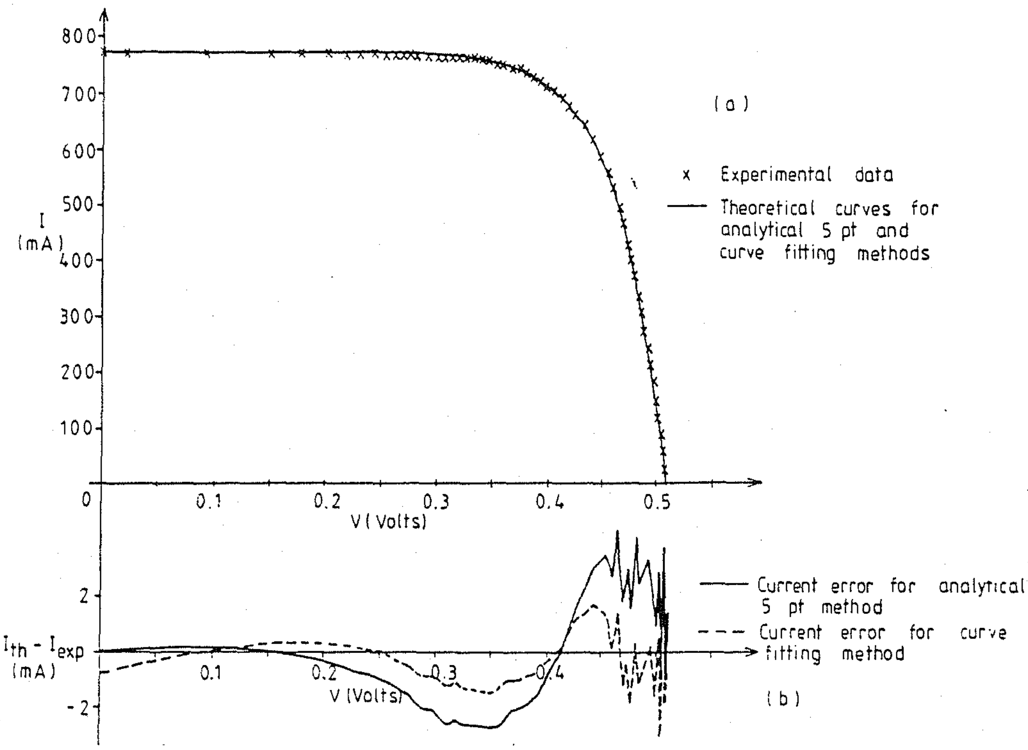

Fig. 5. (a) Comparison of experimental data (data code SN1) with the $I-V$ characteristics generated from parameters extracted with the analytical 5 point and curve fitting methods. (b) Plot of the current deviation of the theoretical $I-V$ characteristics from the experimental data (data code SN1).

given above, it is evident that R_{sh} should be very close to R_{sho} for most cells, and curve fitting, by using a value of R_{sh} which is much lower than R_{sho}, is actually compensating ~~for~~ errors nearer the maximum power point. These errors, though quite small, are problems inherent in fitting the single diode model to the experimental data. As Fig. 5 shows, the decrease in the value of R_s is in turn a compensation for the decrease in the value of R_{sh}. In Fig. 6(a), ϵ is plotted against R_s for fixed values of the other parameters. Note that R_{sh} for this computation is fixed at 142 Ω which is the value of R_{sho} measured by the small signal method. This graph shows that the minimum ϵ occurs when $R_s = 9.9$ mΩ which is very close to the value of $R_s = 10.3$ mΩ obtained by the analytical method. The analytical method therefore gives a value of R_s very close to the best fit value when R_{sh} is fixed at R_{sho}.

The graph in Fig. 6(b) gives a plot of ϵ against R_{sh} for fixed values of the other parameters. Here R_s was set at 10.3 mΩ, the value obtained by the analytical method. The minimum value ϵ occurred when R_{sh} was 120 Ω. However the random scatter of the experimental data ought to be considered. From Fig. 5(b), random scatter on average makes up 10% of the current error, implying that a reasonable estimate of the uncertainty in ϵ would also be 10%. This would give from Fig. 6(b) an R_{sh} range of 90–180 Ω. Thus curve-fitting is an extremely insensitive method of determining R_{sh}. This is because, apart from its effect on the short circuit region, this parameter has negligible influence on other parts of the characteristic.

It can be seen therefore that the curve fitting method produces values of R_{sh} different from the 5-point method because of small deviations in the cell characteristics from ideal single diode behaviour. Curve fitting allows all five parameters to vary interactively while optimising the overall fit, and, because the theoretical current values are relatively insensitive to variations in R_{sh}, the fitting process produces large changes in R_{sh} to accommodate relatively small current errors in other parts of the characteristic, resulting in compensating changes in the final value of R_s. Errors are thus introduced in the final values of both R_s and R_{sh}. The 5-point methods, by measuring the short and open circuit slopes of the characteristic, give more reliable values for both shunt and series resistances.

The accuracy of the analytical method is also dependent on the accuracy with which the 5 data points are measured. The slopes, in particular, the short circuit slope, are more difficult to determine accurately than the other data points. However, the small signal method enabled R_{sho} to be determined to about 10% accuracy and the results show that this is sufficient to give accurate parameter values. The series resistance of the two cells in Table 1 were 10 and 20 mΩ, respectively, while their shunt resistances were 100 and 20Ω, respectively. It is expected

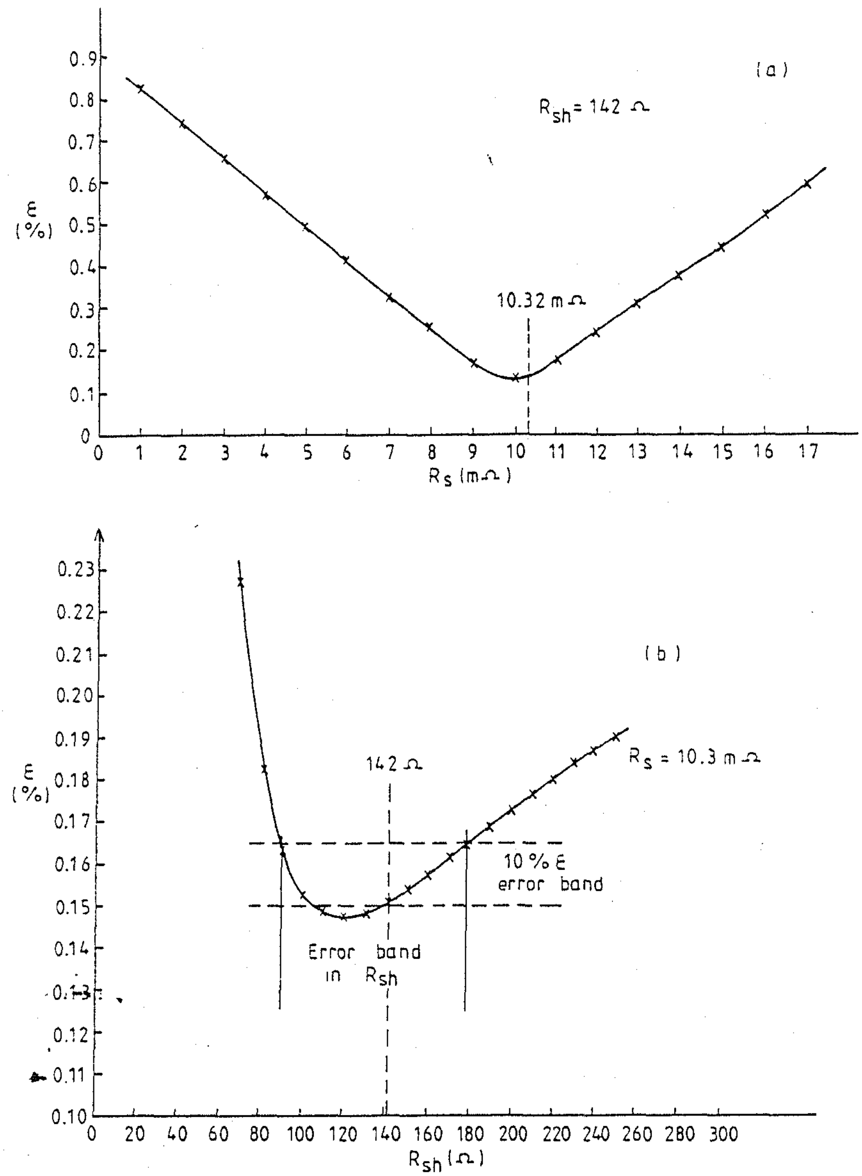

Fig. 6. (a) Plot of ϵ for different R_s values with all the other parameters held at the values obtained from the analytical 5-point method (data code SN1). (b) Plot of ϵ for different R_{sh} values as in (a).

that cells with larger R_s and smaller R_{sh} would have slopes which are easier to measure accurately, and thus pose less of a problem to the analytical method.

All three parameter recovery methods gave negative values of R_s at low illuminations (as shown in Table 1). This would seem to indicate that the one diode model does not give a good description of cell behaviour at low illuminations. Negative resistance values have been also reported by Bryant and Glew [6] for CdS cells.

5. CONCLUSIONS

The analytical 5-point method for the extraction of parameters in a single diode model is shown to give accurate reliable results in situations where the model is an accurate description of cell performance. This method gives parameter values which are very similar to those obtained by curve fitting techniques, but is a faster and more convenient method for parameter extraction. The single diode method is found to give an accurate description of cell performance at illuminations above half AM1, but gives non-physical values at low illuminations.

Acknowledgements—The authors would like to thank Mrs. S. N. Ho and Miss Musni bte Hussain for their technical assistance throughout this work.

REFERENCES

1. M. Wolf and H. Rauschenbach, *Advanced Energy Conversation* 3, 455 (1963).
2. J. C. H. Phang and D. S. H. Chan, *IEEE Trans. Electron Dev.* **ED-31**, 717–718 (1984).
3. K. Rajkanan and J. Shewchun, *Solid-St. Electron.* **22**, 193 (1979).

4. G. L. Araujo and E. Sanchez, *IEEE Trans. Electron Dev.* **ED-29**, 1511 (1982).
5. D. S. H. Chan and J. C. H. Phang, *IEEE Trans. Electron Dev.* **ED-31**, 381–383 (1984).
6. F. J. Bryant and R. W. Glew, *Energy Conversion* **14**, 129 (1975).
7. R. T. Otterbein, D. L. Evans and W. A. Facinelli, 13th IEEE Photovoltaic Specialists Conf. 1074 (1978).
8. G. L. Araujo, E. Sanchez, and M. Marte, *Solar Cells* **5**, 199 (1982).
9. K. L. Kennerud, *IEEE Trans. Aerosp. Electr. Syst.* **AES-5**, 912 (1969).
10. J. P. Charles, M. Abdelkrim, Y. H. Muoy and P. Mialhe, *Solar Cells* **4**, 169 (1981).
11. A. Braunstein, J. Bany and J. Appelbaum, *Energy Conversion* **17**, 1 (1977).
12. M. Wolf, G. T. Noel and R. J. Stirn, *IEEE Trans. Electron Dev.* **ED-24**, 419 (1977).
13. J. C. H. Phang, D. S. H. Chan and J. R. Phillips, *Electron. Lett.* **20**, 406 (1984).

Solar Cells, *14* (1985) 61 - 81

PHOTOVOLTAIC MEASUREMENTS

S. ASHOK

Department of Engineering Science and Mechanics, The Pennsylvania State University, University Park, PA 16802 (U.S.A.)

K. P. PANDE

Bendix Aerospace Technology Center, Allied Corporation, 9140 Old Annapolis Road, Columbia, MD 21045 (U.S.A.)

(Received July 13, 1984; accepted August 20, 1984)

Summary

In this article the commonly used techniques for measurement and evaluation of solar cell devices and materials are reviewed. Topics covered include determination of the solar cell performance parameters under simulated solar illumination, the electrical characteristics to obtain internal device parameters, the spectral response and quantum efficiency, the minority carrier lifetime and diffusion length, and the surface recombination velocity. The merits and limitations of the techniques are also discussed.

1. Introduction

There has recently been remarkable activity in terrestrial photovoltaic research, with a wide range of materials systems under current development. The performance of solar cells depends critically on the properties of the semiconductor materials as well as the nature of the photovoltaic barrier interface. Apart from evaluating the solar cell performance under simulated radiation, it is necessary to measure the basic material and interface parameters in order to assess the scope for further improvement in cell efficiency. In this review a number of techniques used toward this end are described and their advantages and limitations discussed. Starting with a development of the basic equivalent circuit of the solar cell, the experimental procedures for evaluating the performance as well as the internal interfacial parameters are described. Then the techniques for measuring the material parameters of greatest significance to solar cells, *i.e.* minority carrier lifetime, diffusion length and surface recombination velocity, are discussed in detail. The survey is by no means exhaustive, but it is of general applicability to the characterization of a diverse range of solar cell structures.

0379-6787/85/$3.30

2. Basic solar cell structure and equivalent circuit

Figure 1 shows a schematic diagram of a typical solar cell structure, comprising a top window layer (with carrier collection grids), a depleted photovoltaic barrier region (p–n homojunction, p–n, n–n$^+$ or p–p$^+$ heterojunction, Schottky barrier, or metal/insulator/semiconductor Schottky barrier) and the principal semiconductor absorber (with back contacts). The photovoltaic barrier separates out the electron–hole pairs photogenerated within a diffusion length on either side of the barrier (as well as within the barrier itself), thus constituting the photocurrent I_{ph}. The net current I flowing through the lead can be written as

$$I = I_{ph}(\phi) - I_{bk}(V) \tag{1}$$

where I_{bk} is a bucking current caused by the partial recombination of photogenerated electron–hole pairs and depends only on the cell voltage V, and I_{ph} is a function only of absorbed photon flux ϕ per unit time. In general I_{ph} may be voltage dependent, while I_{bk} may be a function of illumination, but the simplification of eqn. (1), the so-called superposition principle or shifting approximation, is generally valid except for certain thin film cells such as those based on CdS, and possibly for cells operating at high solar concentration.

The precise expressions for I_{ph} and I_{bk} are functions of material parameters and interfacial boundary conditions and have been derived for a variety of solar cell configurations [1]. For the appropriate choice of device geometry and contact parameters, I_{ph} approaches the maximum theoretical value of the given incident radiation. In contrast, the bucking current I_{bk} may consist of several components in parallel (and some in series) but at the operating range of solar cells only one of these parallel mechanisms is likely to dominate. Almost invariably these bucking current mechanisms have an exponential dependence on voltage V, so that eqn. (1) can be rewritten in the familiar form

$$I = I_{ph} - I_0\left\{\exp\left(\frac{qV}{nkT}\right) - 1\right\} \tag{2}$$

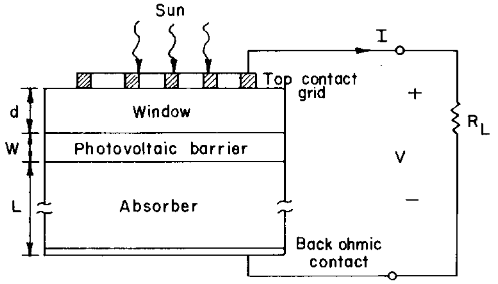

Fig. 1. Schematic diagram of a general solar cell structure.

where I_0 is the saturation current, q the electronic charge, k the Boltzmann constant, T the absolute temperature and $n \geqslant 1$ the so-called "ideality factor". The values of n and I_0 depend strongly on the mechanism of bucking current transport to be discussed in Section 3.3. From eqn. (2) the open-circuit voltage V_{oc} can be written as

$$V_{oc} \approx \frac{nkT}{q} \ln\left(\frac{I_{sc}}{I_0}\right) \tag{3}$$

since the short-circuit current $I_{sc} = I_{ph} \gg I_0$.

The current–voltage (I–V) characteristics of a solar cell in the dark and under illumination are shown in Fig. 2. It is evident that the effect of illumination is a simple vertical shift of the dark I–V characteristic (bucking component) by I_{ph}. The cell efficiency is computed at the maximum power point (V_m, I_m) on the illuminated I–V characteristic as

$$\eta = \frac{V_m I_m}{P_{in}}$$

$$= \mathrm{FF}\,\frac{V_{oc} I_{sc}}{P_{in}} \tag{4}$$

where P_{in} is the input optical power and FF (<1) is the fill factor, which is a measure of the "squareness" of the illuminated I–V characteristic. It can be seen that the fill factor is the ratio of the areas of the two broken rectangles in Fig. 2. It should be noted that the I–V characteristic of a solar cell approaches that of an ideal d.c. power source (an ideal voltage source up to a certain current and an ideal current source beyond) and hence is inherently protected for all passive loading conditions.

It is convenient to represent the solar cell under illumination described by eqn. (2) by means of an equivalent circuit as shown in Fig. 3(a). A more complicated equivalent circuit including the parasitic series resistance R_s (due to bulk and contact resistivity) and the shunt resistance R_{sh} (due to surface leakage and other shunt paths) is indicated in Fig. 3(b). Equations (2) and (3) must now be modified to account for the voltage drop across

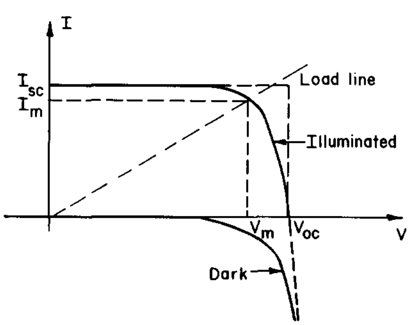

Fig. 2. Solar cell I–V characteristics in the dark and under illumination.

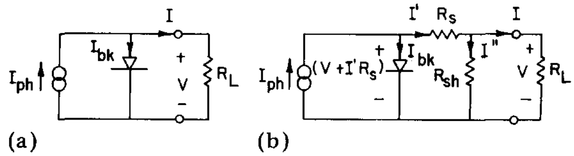

Fig. 3. (a) Simplified equivalent circuit of a solar cell; (b) equivalent circuit with series resistance R_s and shunt resistance R_{sh}.

R_s and the current through R_{sh}. R_s and R_{sh} will affect all the cell performance parameters, but for the usual values encountered in practical cells they contribute mainly to a reduction in the fill factor (see Section 3).

3. Current–voltage characteristics

The I–V characteristics under illumination provide the essential performance parameters of a solar cell, *i.e.* the open-circuit voltage V_{oc}, the short-circuit current I_{sc}, the fill factor FF and hence the cell efficiency. In addition, the I–V characteristics taken in the dark, particularly with temperature as a parameter, are very useful in identifying the limiting recombination mechanisms in the cell as well as in evaluating the internal cell parameters such as the series resistance R_s, the shunt resistance R_{sh}, the diode ideality factor n and the dark or bucking saturation current I_0.

3.1. Cell performance parameters

The illuminated I–V characteristics are most conveniently determined with a solar simulator, since terrestrial solar irradiance is highly variable depending on the location of the laboratory, the season, the time of day, the cloud cover etc. For terrestrial applications the spectrum chosen is usually air mass (AM) 1, corresponding to normal incidence, or AM 2, corresponding to oblique incidence at an angle $\theta = 60°$ between the Sun and the zenith, so that the thickness of the air mass penetrated with AM 2 is twice that of normal incidence (AM X corresponds to $X = \sec\theta$). For space applications the spectrum used is referred to as AM 0 and accurate measurements on such solar cells are often carried out in high altitude balloons and jet aircrafts. Figure 4 shows the solar energy spectrum for AM 0 and AM 2 conditions [1], and Table 1 lists the approximate values of solar irradiance for the typical solar spectra encountered [1].

It is obvious that any light source used for solar simulation in the laboratory must have a spectral distribution which closely matches that of the solar spectrum of interest. A number of schemes involving high power lamps and suitable filters are available, some of them as commercial units. However, it is virtually impossible to match the solar spectrum exactly and so the use of calibrated reference cells furnished by Government agencies such as the National Aeronautics and Space Administration (NASA) and the Jet Propulsion Laboratory is resorted to. A relatively simple *terrestrial*

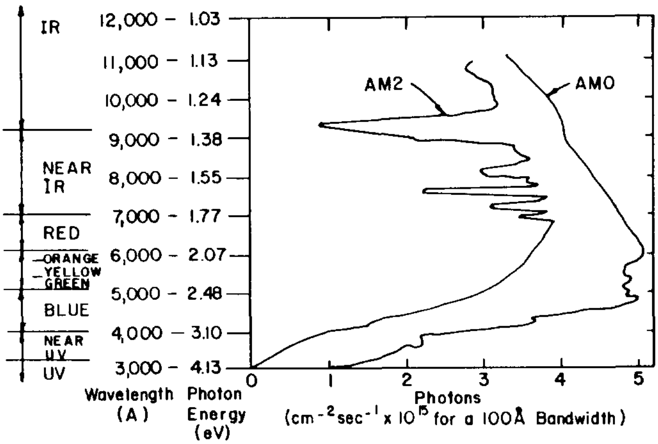

Fig. 4. Solar energy spectrum under AM 0 and AM 2 conditions.

TABLE 1

Approximate value of solar irradiance at various insolations

Air mass	*Solar power density* (mW cm^{-2})
AM 0	135
AM 1	100
AM 2	75

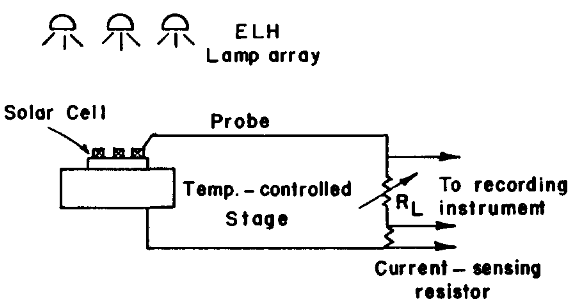

Fig. 5. Schematic diagram of a simple test structure for illuminated I–V measurements.

simulator illustrated schematically in Fig. 5 employs an array of ELH quartz halogen lamps [2]. A NASA cell is used in place of the cell to be evaluated and the lamp voltage is adjusted to obtain the calibration value of the short-circuit current from the reference cell. Subsequently, the illuminated I–V characteristics of the test cell for the chosen AM X spectrum may be traced on an x–y recorder by varying R_L from zero to infinity, or by connecting a semiconductor curve tracer across the cell. It is important to keep the cell temperature at a constant reference value (300 K) and for this purpose it is desirable to mount the cell on a temperature-controlled stage, preferably using a thermoelectric module so that cooling is possible. In choosing a reference cell, the most important criterion is that the spectral response of the reference cell matches that of the test cell, so that accurate measurements can be made with any simulator [2]. However, because of the enormous diversity of solar cell materials and devices under current development, use of the standard silicon reference cells for simulator calibration can result in considerable errors, principally in the measured short-circuit current and efficiency. An accurate, though cumbersome, alternative is to use an absolute efficiency measurement by determining the quantum efficiency of the cell as a function of wavelength (Section 4) and then convoluting it with the appropriate solar insolation [3, 4]. The use of an absolute efficiency measurement also easily lends itself to computer-assisted measurement and evaluation.

The values of V_{oc} and I_{sc} are readily obtained from the x–y recorder or curve tracer plots as the x axis and y axis intercepts respectively. The maximum power point (V_m, I_m) can be obtained by iteration or by using an automatic plotter to plot $P = VI$ *versus* V or I from which $P_m = V_m I_m$ can be determined [5]. It is also possible to digitize the entire illuminated I–V data and to process it to obtain the fill factor FF and the power efficiency η (compare eqn. (4)). The input power density P_{in} is known for the simulated solar insolation (Table 1). In reporting the short-circuit current density $J_{sc} = I_{sc}/A$ and η, it is necessary to specify the area A of the cell so that the contribution of any possible peripheral collection of minority carriers (within a diffusion length of the cell periphery) can be ascertained. Also, the top collection grids used in many experimental cells are not optimized and so J_{sc} and η are often reported excluding the area shaded by the thick metal grid lines (the so-called "active-area" short-circuit current and efficiency). The active-area efficiency evidently projects an optimistic value, so it is useful to state also the "engineering efficiency" which includes the total (exposed as well as shaded) cell area in the computation of J_{sc}. For measurements on concentrator cells a flash technique is most convenient as this minimizes cell heating [6].

3.2. Cell internal parameters

Apart from measuring the above external performance parameters of the solar cell, it is also necessary to determine the internal parameters such as R_s, R_{sh}, η and I_0 since the external performance parameters are dictated by the internal parameters and the internal parameters in turn are related to the material and interface properties. n and I_0 are best evaluated from the bucking or dark I–V characteristics (to be discussed next), while R_s and R_{sh} may be obtained from the illuminated I–V plot itself. From Fig. 3(b) and eqn. (2) modified to account for R_s and R_{sh}, it can be readily shown that R_s is approximately given by the negative inverse slope of the illuminated I–V plot at $I = 0$ (open-circuit point) and R_{sh} by the value at $V = 0$ (short-circuit point). R_s and R_{sh} primarily affect the fill factor which is also dependent on V_{oc}. The series resistance is usually the limiting factor

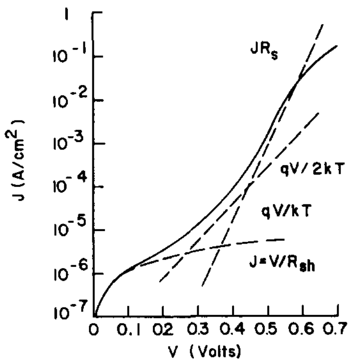

Fig. 6. An illustrative bucking (log J)–V plot, indicating the effect of series resistance R_s, shunt resistance R_{sh} and two distinct bucking current mechanisms (R_s = 0.4 Ω cm^2; R_{sh} = 100 kΩ cm^{-2}; T = 27 °C).

on the fill factor of a single-crystal solar cell, particularly those cells which operate at high solar concentration levels, whereas in thin film and polycrystalline cells the shunt resistance (due to pinholes or grain boundaries) can influence the fill factor and hence η significantly. The presence of series resistance and shunt resistance in cells can be seen most clearly by observing the linear I–V characteristics (on a curve tracer for instance) at low current and high current respectively. The influence of R_s and R_{sh} on the bucking current characteristics is shown on a representative plot in Fig. 6 [7]. It should be noted that the current density scale is logarithmic.

3.3. *Bucking or dark current–voltage characteristics*

The dark or bucking J–V characteristics when evaluated as a function of temperature and plotted on a semilogarithmic scale (Fig. 7) can be extremely useful in identifying the recombination mechanisms and hence the potential improvement in V_{oc} (compare eqn. (3)). The (log I)–V characteristics are most easily obtained by using a logarithmic picoammeter such as the Keithley 26000 unit in series with a voltage ramp and the solar cell in the dark. The analog output of the picoammeter and the voltage ramp can drive an x–y recorder, thereby sweeping out a (log I)–V plot.

The ideality factor n and the saturation current I_0 can be evaluated from the linear regions of the (log I)–V plot by using the slope (inverse slope is approximately equal to $60n(T/300)$ mV per decade of current) and by extrapolating the straight line to zero voltage respectively.

All the common bucking current mechanisms have the exponential dependence of eqn. (2), and their voltage and temperature dependence are indicated in Table 2 [8].

All the various recombination mechanisms listed in Table 2 occur in parallel and one or more of them may be dominant in a given solar cell. For example, in the characteristics of Fig. 6, space charge region recombination is the likely mechanism at low voltages (since n = 2), while minority carrier bulk diffusion dominates at higher forward voltages (until

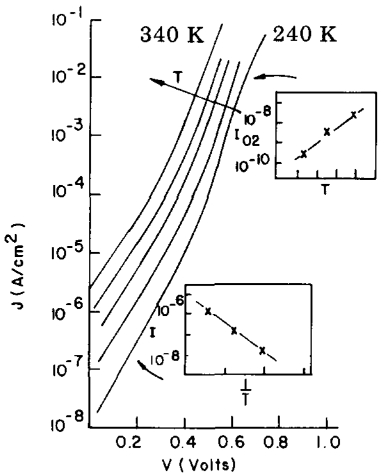

Fig. 7. Bucking current characteristics of a solar cell as a function of temperature dependence of saturation currents I_{01} and I_{02} in the two regions.

it is limited by R_s). The minority carrier bulk diffusion sets the ultimate limit on the maximum V_{oc} obtainable from a solar cell, and hence attempts are made to suppress or eliminate all the other bucking current components in designing the optimal cell with a given materials system.

The $(\log J)$–V plots of Fig. 7, where temperature T is used as a parameter, allow less ambiguous identification of the dominant bucking current mechanisms at different voltage or current ranges since now the temperature dependence of n and I_0 is also available. In the low voltage regime of this representative plot, n is a constant (>1) and I_0 is thermally activated ($\exp(-E/kT)$ dependence (see Fig. 7, lower inset)), thus suggesting space charge recombination (confirmable from the slope of the $\log I_0$ *versus* $1/T$ plots; compare Table 2). In contrast, in the higher voltage regime the plots are parallel to each other; the temperature-independent slope suggests tunneling, which is confirmed by the $\log I_0$ *versus* T plot of Fig. 7, upper inset. Apart from the $(\log I)$–V–T plots, it may be necessary to obtain augmenting data such as from capacitance–voltage (C–V) and internal photoemission measurements in order to pinpoint the bucking current mechanism [9]. A detailed discussion of these techniques is beyond the scope of this paper.

Apart from the classical bucking currents outlined in Table 2, there can also be other competing mechanisms such as Auger recombination (in heavily doped materials) [7], transport through and across grain boundaries (in polycrystalline materials) [10] and space-charge-limited current flow (in amorphous and organic semiconductors) [11]. Also in certain materials systems the bucking current counteracting the photocurrent under illumination may be different from the cell forward current measured in the dark, *i.e.* the superposition principle is not valid. In such instances, the dark I–V characteristics are not useful in predicting the cell performance under

TABLE 2

Bucking current mechanisms and their functional dependence on voltage and temperature

Mechanism	n	I_0	*V dependence*	*T dependence*
Bulk diffusion–recombination	1	constant $\times\, T^3 \exp\left(-\frac{E_g}{kT}\right)$	$\exp\left(\frac{qV}{kT}\right)$	$\exp\left(-\frac{E_g}{kT}\right)$
Space charge region generation–recombination	$1 < n \leqslant 2$	constant $\times\, T^{3/2} \exp\left(-\frac{E_g}{2kT}\right)$	$\exp\left(\frac{qV}{nkT}\right)$	$\exp\left(-\frac{E_g}{2kT}\right)$
Thermionic emission	$\geqslant 1$	constant $\times\, T^2 \exp\left(-\frac{\phi_B}{kT}\right)$	$\exp\left(\frac{qV}{nkT}\right)$	$\exp\left(-\frac{\phi_B}{kT}\right)$
Thermionic-assisted tunneling	$n = n(T) > 1$	$\approx \exp\left(-\frac{\phi_B}{nkT}\right)$	$\exp\left(\frac{qV}{nkT}\right)$	$\exp\left(-\frac{\phi_B}{nkT}\right)$
Direct or trap-assisted tunneling	nT = constant	$\exp\left(\frac{T}{T_0}\right)$	$\exp\left(\frac{V}{V_0}\right)$	$\exp\left(\frac{T}{T_0}\right)$

illumination and the I–V measurements may have to be modified with the use of a bias light source or by obtaining I_{sc}–V_{oc} data with illumination level as a parameter [12].

4. Spectral response and quantum efficiency

The spectral response shows the relative contribution of photons of different energy to the short-circuit photocurrent of the solar cell. The external quantum efficiency η_{ext} is defined as

$$\eta_{ext}(\lambda) = \frac{I_{sc}(\lambda)}{q\phi(\lambda)} \qquad (5)$$

where $\phi(\lambda)$ is the photon flux per second at wavelength λ incident on the cell and $I_{sc}(\lambda)$ is the measured short-circuit current. Thus a plot of η_{ext} against λ will give the absolute spectral response, which when folded with the appropriate solar spectrum will yield the total short-circuit photocurrent of the cell. The solar cell spectral response is determined by a number of factors including the optical absorption coefficient $\alpha(\lambda)$, the minority carrier diffusion length l, the absorber length L, the surface recombination velocity S, the type of photovoltaic barrier (homojunction, heterojunction or Schottky barrier) and the presence of antireflection coatings. Hence, spectral response measurements can be extremely useful in assessing the performance of the cell and in gaining insight for future design improvement.

The schematic diagram of a basic spectral response measurement set-up is shown in Fig. 8. It consists of a polychromatic light source such as a tungsten–halogen or xenon lamp, a monochromator spanning the spectral range of interest (350 - 1100 nm), a light chopper for synchronous or lock-in detection, a calibration detector and a lock-in amplifier. The detector may be a "black" detector such as a thermopile or a silicon diode detector probe used in conjunction with a photometer such as the EG & G model 550

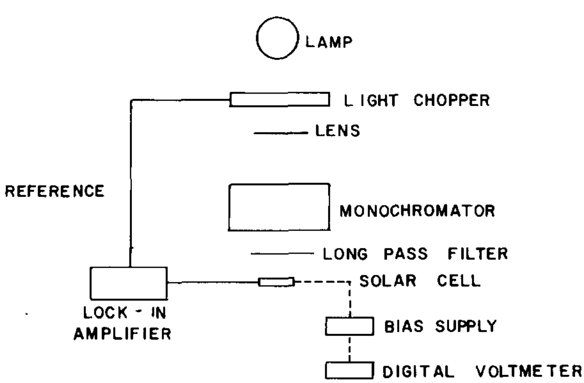

Fig. 8. Schematic diagram of a set-up for spectral response and quantum efficiency measurements.

or the Tektronix J16. By measurement of the solar cell short-circuit photocurrent as a function of wavelength as well as the detector output at each wavelength and conversion of the detector output at each wavelength into photon flux per unit time, the quantum efficiency can be determined over the wavelength range of interest.

It may also be convenient to determine the absolute quantum efficiency at a single wavelength (by using a laser and a pyroelectric detector, for example), and then to use it to normalize the relative response data of the detector. If only the relative spectral response is desired, then the absolute calibration factor of the detector is not needed and it is very convenient to use a thermopile whose response is practically flat over the spectral range of interest for solar cells. The spectral response quantum efficiency measurement systems may be readily automated for rapid evaluation of cell performance [3].

A simple alternative to the use of a monochromator with its attendant small illumination level is to substitute it with a batch of several narrow bandpass interference filters (filter wheel) [13, 14]. The values of η of some thin film cells such as the Cu_2S/CdS cell and cells made on many amorphous and organic semiconductors are dependent on the illumination level, and hence the spectral response measurement of these cells must be carried out at levels comparable with those in the actual solar spectrum used. The same argument holds true for concentrator cells operating at high concentration levels (more than 100 suns). A photographic flash-lamp may be used as a pulsed-light source, which also minimizes the risk of overheating the interference filters used [13]. It is also possible to use a "white light" bias source and a small-signal chopped monochromatic source (of variable λ) to carry out spectral response measurements at high light intensities.

5. Diffusion length

The minority carrier diffusion length $l = (D\tau)^{1/2}$ (where D is the diffusion constant and τ is the lifetime) is the single most important material parameter of a solar cell, as it determines the photocurrent and also the limiting value of the bucking current and hence the open-circuit voltage. The three most commonly used techniques for diffusion length measurement are as follows.

5.1. Spectral response measurements

Diffusion length measurement from spectral response data is most easily carried out with a Schottky barrier device, using a semitransparent (thickness, approximately 100 Å) metal film. For illumination from the top, the short-circuit photocurrent is approximately given by [15]

$$I_{sc} \approx q\phi(\lambda)T(\lambda)\left\{1 - \exp(-\alpha W) + \frac{\alpha l}{1 + \alpha l}\exp(-\alpha W)\right\} \qquad (6)$$

where $\phi(\lambda)$ is the incident photon flux per second, $T(\lambda)$ is the transmission through the upper metal layer, $\alpha(\lambda)$ is the absorption coefficient in the semiconductor, l is the minority carrier diffusion length and W is the width of the depletion region. Equation (6) is valid for a long diode ($L \gtrsim 3l$) over a range of λ for which there is strong absorption in the semiconductor ($L \gtrsim 3(1/\alpha)$).

In the classical method of obtaining l from spectral response the short-circuit photocurrent is measured as a function of λ over a range wherein $\alpha(\lambda)W \ll 1$.

Then eqn. (6) may be simplified to

$$\left\{\frac{I_{sc}}{q\phi(\lambda)T(\lambda)}\right\}^{-1} = \frac{1}{l}\left\{l + \frac{1}{\alpha(\lambda)}\right\} \tag{7}$$

Thus a plot of the inverse of the short-circuit photocurrent per incident photon (in the semiconductor), *i.e.* the inverse quantum efficiency, against $1/\alpha(\lambda)$ will yield a straight line with a horizontal axis intercept of magnitude equal to the diffusion length. While conceptually simple, this method suffers from the need to know the precise values of the photon flux incident on the cell and the transmission coefficient T of the Schottky metal. Of course, if the assumptions leading to eqn. (6) are not valid, l can be deduced from the measured spectral response by curve fitting to exact theoretical expressions (including the effect of back-surface recombination velocity [16, 17]).

Many of the problems associated with the above technique may be obviated by using a single wavelength for which the absorption length $1/\alpha(\lambda)$ is of the order of the depletion width W and varying W by applying a reverse bias on the Schottky barrier [18, 19]. Hence, eqn. (6), subsequent to normalization at an arbitrary depletion width W_0, may be written as

$$\begin{aligned} I_{norm}(\alpha W) &= \frac{I_{sc}(W)}{I_{sc}(W_0)} \\ &= \frac{1 + \alpha l - \exp(-\alpha W)}{1 + \alpha l - \exp(-\alpha W_0)} \end{aligned} \tag{8}$$

The depletion width $W(V)$ may be determined as a function of reverse voltage V by using high frequency (1 MHz) capacitance measurements:

$$W(V) = \frac{\epsilon A}{C(V)} \tag{9}$$

where ϵ is the dielectric permittivity of the semiconductor, A is the diode area and $C(V)$ is the depletion capacitance. It should be noted that there is no need to calibrate the photon flux or to know the value of transmission through the metal film. The diffusion length may be obtained by matching the experimental plot of I_{norm} *versus* $\alpha(\lambda)W(V)$ to the expression of eqn. (8). This method is particularly amenable to direct gap materials such as GaAs that have relatively short diffusion lengths (1 - 10 μm). It is pertinent to note that in either of the techniques outlined above the value of the absorption coefficient of the absorber semiconductor must be known as a function of λ. Empirical expressions for $\alpha(\lambda)$ based on experimental results are available for silicon [20] and may be used for evaluating single-crystal silicon cells.

A simplification of the second technique is possible when the absorption coefficient is so small at the illuminated wavelength that $\alpha W \ll 1$. Then eqn. (6) reduces to

$$I_{sc}(V) = \frac{q\phi(\lambda)T(\lambda)}{1 + l\alpha(\lambda)}\alpha(\lambda)\{W(V) + \alpha\} \qquad (10)$$

Since $W(V)$ can be obtained from C–V measurements (compare eqn. (9)), a plot of I_{sc} against W (with reverse voltage V as the variable parameter) should yield a straight line with intercept l [18]. In this modified technique it is not necessary to know the exact value of $\alpha(\lambda)$ but simply to choose a wavelength λ such that the product $W(V)\alpha(\lambda) \ll 1$.

5.2. Surface photovoltage measurements

The surface photovoltage method depends on the spectral dependence of the open-circuit voltage developed at the surface of the semiconductor. The surface photovoltage may be capacitively sensed and hence there is no inherent need to form a permanent or semipermanent photovoltaic junction such as a p–n junction or a Schottky barrier. The increase in minority carrier concentration under illumination reduces the surface band bending (formed initially as a result of surface states or a junction) and thereby causes the photovoltage. The measurement set-up is basically the same as that used for spectral response; the surface is illuminated with a chopped monochromatic radiation of $h\nu > E_g$ and the surface photovoltage is sensed with a capacitive probe such as that illustrated in Fig. 9. Under the conditions $W < 1/\alpha < L$ and $l \ll L$, and if the excess minority concentration under illumination is far less than the majority carrier concentration, the surface photovoltage SPV is a function of the excess minority carrier concentration and may be written as [21]

$$\mathrm{SPV} = \mathrm{f}\left(\mathrm{constant} \times \phi\,\frac{1}{1/\alpha + l}\right) \qquad (11)$$

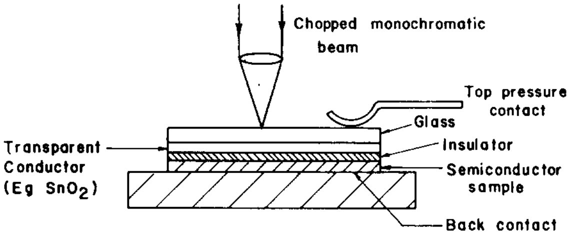

Fig. 9. Schematic diagram of a test structure for surface photovoltage measurements.

Hence a plot of the relative photon flux against the inverse absorption coefficient at constant SPV (by feedback control in the experimental set-up, if so desired) will yield a straight line, the negative x axis intercept of which yields the diffusion length. The method is relatively insensitive to surface recombination and can be easily used to map the diffusion length profile of semiconductor wafers and hence to diagnose the presence of inhomogeneities. However, considerable errors are observed when the beam diameter is reduced below about $30l$, apparently as a result of lateral diffusion of photogenerated carriers and their recombination in the semiconductor bulk and/or the surface [22].

The surface photovoltage technique is particularly attractive for highly absorptive materials and it has recently been used to measure the ultrashort diffusion length of holes in hydrogenated amorphous silicon (a-Si:H) alloy [23]. Figure 10 is a representative surface photovoltage plot for a-Si:H, indicating a diffusion length of 0.17 μm. In highly photoconductive materials such as a-Si:H the diffusion length is a function of illumination and so the surface photovoltage may be detected with a.c. coupling under a superposed bias light or alternatively with a vibrating Kelvin probe [23] or a liquid Schottky barrier [24].

5.3. Beam-induced current measurements

The beam-induced current technique essentially uses the impulse response of a photovoltaic junction, the excitation being any high absorption radiation or particle beam such as a laser beam or an electron beam, scanned in a direction perpendicular to the junction. The use of beam-induced current to evaluate the minority carrier diffusion length dates back to 1951 [25] when a light spot from a narrow slit was scanned across a p–n junction and the photocurrent measured as a function of the spot position x from the junction. The idea was extended later on by substituting an electron beam (20 keV) which can be accurately focused (diameter, approximately 1 μm) and scanned across the junction with high

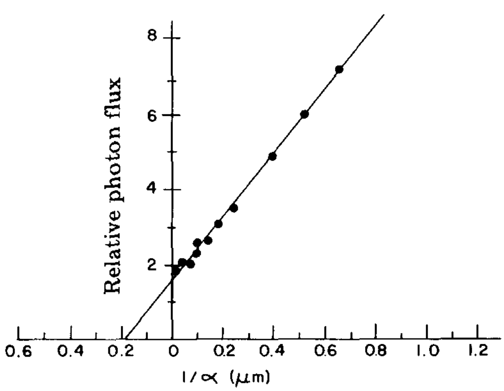

Fig. 10. Example of a surface photovoltage plot to determine the minority carrier diffusion length (l = 0.17 μm).

precision [26]. Thus a scanning electron microscope can be readily adapted for the beam-induced current method and hence the scanning electron microscopy–electron-beam-induced current technique has become standard for evaluating the minority carrier diffusion length l. The advent of the laser with its extremely high directionality and hence narrow beam width has again made it easier to use a scanning light spot and so the laser-beam-induced current technique is also frequently used now to determine l.

The most convenient structure for either of the beam-induced current techniques is a Schottky barrier with the beam scanned perpendicular to the junction as shown in Fig. 11(a). For beams that penetrate negligibly into the bulk of the semiconductor ($\alpha x > 1, \alpha l > 1$) the short-circuit photocurrent I_{sc} due to the diffusion of minority carriers from beam position x toward the junction varies asymptotically as [26]

$$I_{sc} \propto \exp\left(-\frac{x}{l}\right) \tag{12}$$

for $x > l$ and uniform surface recombination velocity S. Hence l can be evaluated readily from the straight line plot of $\log I_{sc}$ *versus* x as

$$l = \left|\frac{\mathrm{d}\{\ln(I_{sc})\}}{\mathrm{d}x}\right|^{-1} \tag{13}$$

It should be noted that the location of the junction, *i.e.* $x = 0$, is easily found from the peak of I_{sc} *versus* x. More accurate expressions for I_{sc} should be used and l is deduced from curve fitting the measured data if the above assumptions are not valid over an appreciable range of the scan distance x [27]. An illustrative scanning electron microscopy–electron-beam-induced current plot is shown in Fig. 11(b). A major disadvantage of scanning in a direction perpendicular to the junction is the precision with which the beam

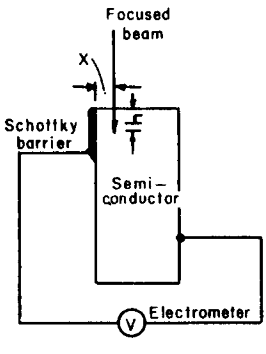

(a)

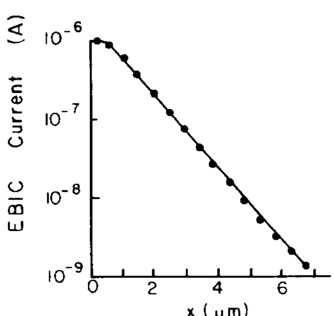

(b)

Fig. 11. (a) Illustration of a test structure for diffusion length measurement by beam-induced current; (b) illustrative electron-beam-induced current (EBIC) plot (l = 0.90 μm).

position should be known, and this is particularly difficult for materials with short diffusion lengths ($l = 1$ - 5 μm). An attractive alternative is to use an angle-lapped junction, as shown in Fig. 12(a), where a geometric amplification is provided by the very small lapping angle θ (giving a geometric "gain" of $1/\sin\theta$). Provided that the other assumptions are valid, eqn. (12) is still valid, since at any beam position z from the junction intersection at the lapping surface, the vertical distance x to the junction equals $z \sin\theta$. However, it is the relatively large value z that is now actually measured in the experimental set-up. It may be observed that by using a p–n junction both the electron and the hole diffusion lengths (in the p region and the n region respectively) can be deduced by angle lapping both the top and the bottom side of the semiconductor wafer.

A third modification of the structure suitable for beam-induced current measurements is indicated in Fig. 12(b) [28]. This has the advantage that the beam is incident normal to the collecting junction (a Schottky barrier, for instance) and is at a lateral distance x from the edge of the junction. For this case the short-circuit photocurrent I_{sc} has been shown to be [28]

$$I_{sc} \propto \frac{\exp(-x/l)}{x^{3/2}} \tag{14}$$

provided that $l \ll x$ and that the depletion region width W beneath the surface is such that $W \ll h$ and $h \ll x$ where h is the location beneath the surface of the ideal beam-induced point source for electron–hole pair generation. Thus, the diffusion length can be deduced from the slope of the linear $\ln(I_{sc}x^{3/2})$ *versus* x plot.

The beam-induced current technique may be readily modified to measure simultaneously the minority carrier lifetime with high spatial resolution by modulating the beam with an a.c. signal [29, 30]. The simple analytical expressions used above may need modification when the simplifying assumptions are not valid. Theoretical treatments that account for high level injection [31], surface recombination [32] and generation volume distribution (non-point source) [33] are available in the literature to enable accurate evaluation of l. It may be noted that apart from electron and photon beams any narrowly focused particle beam (*e.g.* α particles)

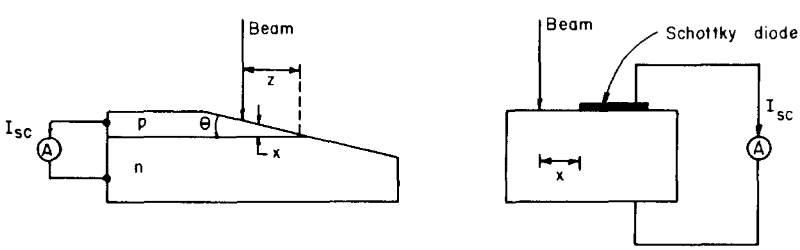

(a) (b)

Fig. 12. Illustrations of alternate test structures for beam-induced current measurements: (a) angle-lapped p–n junction; (b) Schottky barrier with lateral carrier collection.

that can create electron–hole pairs in the semiconductor may be used in the beam-induced current technique.

6. Minority carrier lifetime

For evaluating solar cell materials it is generally preferable to measure the minority carrier diffusion length directly by any of the techniques described above. However, it is often convenient to measure the carrier lifetime τ with a relatively simple experimental set-up and then to infer l indirectly by assuming the value of diffusion coefficient D ($l = (D\tau)^{1/2}$). The two basic lifetime measurement techniques are as follows.

6.1. Diode reverse recovery

This is the standard technique to evaluate the response time of any semiconductor diode and consists of pulsing a diode from forward to reverse bias and observing the transient; the decay time is a measure of the minority carrier lifetime [34]. However, this technique is unsuitable for Schottky barrier solar cells (or test structures) since there is no appreciable minority carrier storage in these majority carrier devices.

6.2. Open-circuit voltage decay method

This is the recommended method for solar cells and is suitable for p–n junction as well as Schottky barrier cells. Figure 13(a) shows a schematic diagram of a photo-induced open-circuit voltage decay measuring circuit, where a flash pulse (with a very short fall time) from a stroboscope generates photocarriers in the cell and the subsequent decay of the open-circuit voltage V_{oc} is monitored on an oscilloscope. Figure 13(b) is a sketch of the decay of V_{oc} with time, with two linear regions (I and II) and a non-linear region (III) corresponding to high level injection (in which the excess minority carrier concentration exceeds the thermal equilibrium majority carrier concentration), intermediate injection (in which the excess minority carrier concentration exceeds the equilibrium minority carrier concentration) and low level injection (in which the excess minority carrier

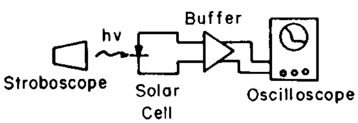

(a)

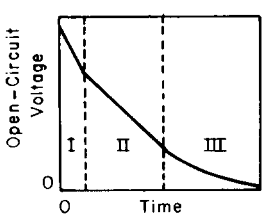

(b)

Fig. 13. (a) Schematic diagram of a simple test set-up for open-circuit voltage decay measurement of minority carrier lifetime; (b) illustrative open-circuit voltage decay plot indicating three distinct regions.

concentration is less than the equilibrium minority carrier concentration) respectively in the principal absorbing region (base) of the solar cell. Straightforward solution of the minority carrier continuity equation for diffusive transport in the base yields τ as given below [35].

In region I

$$\tau = \frac{2kT}{q}\left(\frac{\mathrm{d}V_{\mathrm{oc}}}{\mathrm{d}t}\right)^{-1} \tag{15}$$

In region II

$$\tau = \frac{kT}{q}\left(\frac{\mathrm{d}V_{\mathrm{oc}}}{\mathrm{d}t}\right)^{-1} \tag{16}$$

and in region III

$$\tau = \frac{kT}{q}\left[\exp\left\{\frac{qV(0)}{kT}\right\} - 1\right] \exp\left(-\frac{t}{\tau}\right) \tag{17}$$

where $V(0)$ is the open-circuit voltage at the termination of the excitation. Thus, this method enables measurement of the lifetime at different injection levels. Equations (15) and (17) are predicated on the assumptions of negligible excess charge in the space charge region and the absence of any contribution to the photovoltage from the top window or emitter layer. Some possible errors associated with this technique, due to the back-surface field contact and the *RC* time constant of the photovoltaic junction, have recently been pointed out, and an alternative method with a d.c. light source added to the injection pulse (flash) has been proposed [36]. Furthermore, in materials with appreciable trap concentration the measured decay time will not be the true minority carrier lifetime but will rather be obscured by the carrier trapping time.

6.3. *Other lifetime measurement techniques*

Other techniques for obtaining the minority carrier lifetime include measuring the change in the free-carrier IR absorption due to the presence of excess free carriers [37] and monitoring the phase shift introduced by the cell on an a.c. signal superimposed on the d.c. input in a beam-induced current scheme [29, 30]. It is important to note that in calculating the diffusion length from lifetime measurements the value of the diffusion constant D, which in turn is deduced from measurements of carrier mobility, is assumed. However, the mobility and hence the diffusion constant are majority carrier values and may not be accurate for minority carriers as required for minority carrier diffusion length calculations. Hence, a direct measurement of the diffusion length as outlined in Section 5 would in general yield a more accurate result.

7. Surface recombination velocity

Recombination of photogenerated minority carriers at surfaces away from the photovoltaic junction can considerably reduce the short-circuit photocurrent, particularly in direct gap semiconductors that have relatively short diffusion lengths and absorption lengths ($1/\alpha$). In high efficiency cells, additional improvement in efficiency is often possible only by reducing the surface recombination with n–n^+ or p–p^+ high–low junctions or lattice-matched heterojunctions or by surface passivation with insulators. The parameter that characterizes surface recombination is the surface recombination velocity S, which is defined as the ratio of the rate of flow of charge carriers into unit surface area to the excess carrier density in the bulk just beneath the surface.

It is practically impossible to isolate the effect of surface recombination from bulk recombination and so an "effective" lifetime or diffusion length is usually measured. In one such technique [38, 39], scanning electron microscopy–electron-beam-induced current, the beam penetration depth h of the electron beam is varied by changing the beam accelerating voltage V_A and the effective diffusion length l_{eff} measured as a function of h (see Fig. 11(a)). The value of h is dependent on the beam voltage and varies as $V_A^{1.7}$. The measured effective diffusion length l_{eff} can be shown to depend on the bulk diffusion length l, the bulk lifetime τ, the surface recombination velocity S and the electron beam penetration depth h as [38]

$$l_{eff}^2 = \alpha^2 \left\{ 1 - \frac{S\tau/l}{1 + S\tau/l} \exp\left(- \frac{h}{l} \right) \right\} \tag{18}$$

As shown for a representative example in Fig. 14, a straight line is obtained if $\ln\{1 - (l_{eff}/l)^2\}$ is plotted against h (or $V^{1.7}$). The intercept of the line with the ordinate yields the term within braces in eqn. (18), and hence the surface recombination velocity S. If the generation source cannot be assumed to be point like and the sample dimensions are not large compared with l, a more accurate analysis is necessary to determine S [40]. Other

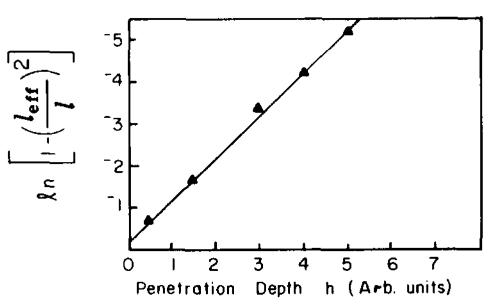

Fig. 14. Illustration of plot to determine the surface recombination velocity from the beam penetration depth h.

techniques for surface recombination velocity measurement include photoluminescence time decay, IR absorption and the photoelectromagnetic effect.

A number of other specialized measurement techniques have been developed to assess the performance of particular solar cell systems and configurations, but for brevity this paper has dealt only with methods of broad applicability.

References

1 S. J. Fonash, *Solar Cell Device Physics*, Academic Press, New York, 1981.
2 C. H. Seaman, B. E. Anspaugh, R. G. Downing and R. S. Estey, *Proc. 14th Photovoltaic Specialists' Conf., San Diego, CA, January 7 - 10, 1980*, IEEE, New York, 1980, p. 494.
3 J. L. Shay, S. Wagner, R. W. Epworth, K. J. Bachmann and E. Buehler, *J. Appl. Phys.*, *48* (1977) 4853.
4 H. B. Curtis, *J. Appl. Phys.*, *50* (1980) 500.
5 Y. W. Lam, *J. Phys. E*, *14* (1981) 1302.
6 E. Fanetti, *Electron. Lett.*, *17* (1981) 469.
7 R. N. Hall, *Solid-State Electron.*, *24* (1981) 595.
8 S. Kar, S. Ashok and S. J. Fonash, *J. Appl. Phys.*, *51* (1980) 3417.
9 S. M. Sze, *Physics of Semiconductor Devices*, Wiley, New York, 1981, p. 286.
10 W. Hwang, E. S. Yang, H. C. Card and C. M. Wu, *Proc. 14th Photovoltaic Specialists' Conf., San Diego, CA, January 7 - 10, 1980*, IEEE, New York, 1980, p. 404.
11 S. Ashok, P. Lester and S. J. Fonash, *IEEE Electron Device Lett.*, *2* (1981) 184.
12 P. Panayatos and H. C. Card, *Proc. IEEE*, *127* (1) (1980) 308.
13 J. C. Larue, in R. Van Overstraeten and W. Palz (eds.), *Proc. 2nd Commission of the European Communities Conf. on Photovoltaic Solar Energy, West Berlin, April 23 - 26, 1979*, Reidel, Dordrecht, 1979, p. 477.
14 N. C. Change and J. R. Sites, *J. Appl. Phys.*, *49* (1978) 4833.
15 R. F. McQuat and D. L. Pulfrey, *Proc. 11th Photovoltaic Specialists' Conf., Phoenix, AZ, May 6 - 8, 1975*, IEEE, New York, 1975, p. 371.
16 H. C. Casey, Jr., B. I. Miller and E. Pinkas, *J. Appl. Phys.*, *44* (1973) 1281.
17 H. J. Hovel, *Proc. 12th Photovoltaic Specialists' Conf., Baton Rouge, LA, November 15 - 18, 1976*, IEEE, New York, 1976, p. 913.
18 M. L. Young and M. C. Rowland, *Phys. Status Solidi A*, *10* (1973) 603.
19 R. J. Lender, S. Tiwari, J. M. Borrego and S. K. Ghandhi, *Solid-State Electron.*, *22* (1979) 213.
20 K. Graff and H. Fisher, in B. O. Seraphin (ed.), *Solar Energy Conversion*, Springer, Berlin, 1979.
21 A. M. Goodman, *J. Appl. Phys.*, *32* (1961) 2550.
22 B. L. Sopori, *Solid-State Electron.*, *23* (1980) 139.
23 J. Dresner, D. G. Szostak and B. Goldstein, *Appl. Phys. Lett.*, *38* (1981) 998.
24 A. R. Moore, *Appl. Phys. Lett.*, *40* (1982) 403.
25 F. S. Goucher, G. L. Pearson, M. Sparks, G. K. Teal and W. Shockley, *Phys. Rev.*, *81* (1951) 637.
26 H. Higuchi and H. Tamura, *Jpn. J. Appl. Phys.*, *4* (1965) 316.
27 K. L. Ashley and J. R. Biard, *IEEE Trans. Electron Devices*, *14* (1967) 429.
28 D. I. Ioannou and C. A. Dimitriadis, *IEEE Trans. Electron Devices*, *29* (1982) 445.
29 T. Fuyuki and H. Matsunami, *J. Appl. Phys.*, *52* (1981) 3428.
30 J. Pietzsch, *Solid-State Electron.*, *25* (1982) 295.
31 S. M. Davidson, R. M. Innes and S. M. Lindsay, *Solid-State Electron.*, *25* (1982) 261.

32 T. Fuyuki, H. Matsunami and T. Tanaka, *J. Phys. D, 13* (1980) 1093.
33 T. Fuyuki, H. Matsunami and T. Tanaka, *J. Phys. D, 13* (1980) 1503.
34 B. G. Streetman, *Solid-State Electronic Devices,* Prentice-Hall, NJ, 1972, p. 184.
35 J. E. Mahan, T. W. Ekstedt, R. I. Frank and R. Kaplow, *IEEE Trans. Electron Devices, 26* (1980) 733.
36 A. R. Moore, *RCA Rev., 40* (1980) 549.
37 R. J. Schwartz and J. L. Gray, *Proc. 12th Photovoltaic Specialists' Conf., Baton Rouge, LA, November 15 - 18, 1976,* IEEE, New York, 1976, p. 83.
38 L. Jastrzebski, L. Lagowski and H. C. Gatos, *Appl. Phys. Lett., 27* (1975) 537.
39 L. Jastrzebski, H. C. Gatos and J. Lagowski, *J. Appl. Phys., 48* (1977) 1730.
40 T. Fuyuki and H. Matsunami, *Jpn. J. Appl. Phys., 20* (1981) 743.